Genetic variation associated with plastic and homeostatic growth responses to drought in Arabidopsis

Running head: Adaptive homeostasis in Arabidopsis drought response

Ángel Ferrero-Serrano[1*] & Sarah M. Assmann[1*]

[1]Biology Department, Penn State University, 208 Mueller Laboratory, University Park, PA, 16802, USA

*** Correspondence:**

Ángel Ferrero-Serrano: aaf11@psu.edu

Sarah M. Assmann: sma3@psu.edu

Highlight

Information on phenotype, genotype, and transcript abundance is integrated to identify candidate plasticity and homeostasis genes and processes associated with local adaptation to drought stress in Arabidopsis accessions of the Iberian Peninsula.

Abstract

Natural genetic variation influences plant responses to environmental stressors. However, the extent to which such variation underlies plastic versus homeostatic response phenotypes has been little studied. We quantified the extent of drought-induced changes in leaf area in a set of Iberian Arabidopsis accessions and then performed association studies correlating plasticity in this phenotype with genomic and transcriptomic variation. Drought-induced plastic reductions in relative leaf area typified accessions originating from productive environments. In contrast, homeostasis in relative leaf area typified accessions originating from unproductive environments. Genome-Wide Association Studies (GWAS), Transcriptome Wide Association Studies (TWAS), and expression GWAS (eGWAS) highlighted the importance of auxin-related processes and, in particular, the potential role of the *SMALL AUXIN UP RNA 26* (*SAUR26*) gene in conferring leaf area plasticity. Homeostatic responses in relative leaf area were associated with a diverse gene set and positively associated with a higher intrinsic water use efficiency (WUE_i), as confirmed in a TWAS metanalysis of previously published $\delta^{13}C$ measurements. Thus, we have identified not only candidate "plasticity genes" but also candidate "homeostasis genes" controlling leaf area. Our results demonstrate the value of a combined GWAS, TWAS, and eGWAS approach to identify mechanisms underlying phenotypic responses to stress.

Keywords: *Arabidopsis thaliana* (Arabidopsis), drought, eGWAS, GWAS, plasticity, transcriptome, TWAS, WUE_i.

Introduction

In the Italian novel The Leopard, one of the main characters famously conveys the idea that 'Everything must change so that everything can stay the same.' Often, there is a cost associated with change that resonates with the plastic developmental responses observed in plants when faced with stress (Bradshaw, 1965; West-Eberhard, 2003). Plasticity marks a departure from a homeostatic state in response to an environmental cue, often followed by "allostatic" responses to return to a homeostatic state (Fig. 1). These allostatic responses involve a myriad of physiological and developmental regulatory processes that stabilize critical aspects of plant physiology. Under repeated stress there is an associated metabolic and physiological cost associated with departure from the optimal state that is not completely alleviated upon return to homeostasis These retained detrimental

54 effects are known as allostatic load (McEwen and Stellar, 1993), with important implications for
55 fitness and survival from an evolutionary standpoint.

56 Stress often elicits plastic responses in plant developmental traits (Dorn *et al.*, 2000; van
57 Kleunen and Fischer, 2005; Forsman, 2015). However, simply because a given trait is plastic does
58 not mean that this plasticity is adaptive (Ghalambor *et al.*, 2007). Plants that are not adapted to stress
59 may exhibit plastic responses that are maladaptive. Under such conditions, homeostasis or lack of
60 plasticity may, in turn, be adaptive (Fig. 1; Ferrero-Serrano and Chakravorty, 2023). This study aims
61 to explore the genetic basis of both plasticity and homeostasis imposed by recurrent drought events
62 during the vegetative development of *Arabidopsis thaliana*.

63 Drought is among the strongest factors driving adaptation in plants (Siepielski *et al.*, 2017;
64 Exposito-Alonso *et al.*, 2019). Since climate projections predict drought events to become more
65 frequent, intense, and unpredictable (Donat *et al.*, 2016), we can expect that drought episodes will
66 become increasingly more difficult for plants to adapt to. For this reason, understanding the genetic
67 basis and adaptation potential of phenotypic traits and their plastic or homeostatic responses to
68 drought is paramount for ameliorating climate change impacts in natural and managed ecosystems.

69 The Iberian Peninsula is a drought-prone region particularly vulnerable to the effects of
70 climate change on precipitation (Vicente-Serrano, 2006a; Vicente-Serrano, 2006b; Coll *et al.*, 2016;
71 Páscoa *et al.*, 2017). The Iberian Arabidopsis population is particularly valuable because its
72 accessions originate from a broad range of environments (Lobo *et al.*, 2001; Rey Benayas and
73 Scheiner, 2002), and previous studies of this population have provided considerable insight into
74 Arabidopsis evolution and development (Picó *et al.*, 2008; Montesinos *et al.*, 2009; Gomaa *et al.*,
75 2011; Méndez-Vigo *et al.*, 2011; Montesinos-Navarro *et al.*, 2011; Picó, 2012; Manzano-Piedras *et*
76 *al.*, 2014; Wolfe and Tonsor, 2014; Vidigal *et al.*, 2016; Exposito-Alonso *et al.*, 2018a; Marcer *et al.*,
77 2018; Castilla *et al*. 2020). In the present study, we utilize GWAS, Transcriptome-Wide Association
78 Studies (TWAS), and Expression Genome-Wide Association Studies (eGWAS) to identify natural
79 genetic and transcript abundance variation underlying both plastic and homeostatic leaf area
80 responses to drought in Iberian Arabidopsis accessions. Leaf area is a vital trait in relation to growth:
81 leaf area production determines the total amount of light intercepted by plants, carbon assimilation,
82 and the extent of evaporative water loss. We uncover an adaptive homeostatic growth strategy in
83 accessions from less productive environments, address its genetic basis, and conclude that phenotypic

homeostasis is under genetic control and of evolutionary importance, just as previously argued for plasticity (Bradshaw, 1965; Via *et al.*, 1995).

Materials and Methods

Plant materials and phenotyping

Seeds for 43 Iberian accessions (Table P1 for the list of accessions) were cold-stratified for four days at 4°C to synchronize germination. Plants were grown in 10 cm square pots containing Metro-mix 360 potting mixture (Sun Gro Horticulture Canada Ltd) in a greenhouse with an average daytime 500 μmol $m^{-2}s^{-1}$ photosynthetic photon flux density (PPFD) (8h light: 16h dark, with light supplied as natural daylight supplemented with 1000W metal halide lamps) and average day/night temperatures of 22°C /20°C.

For each Iberian accession, we grew one plant per pot, with five replicates for each of the control and drought treatments (10 plants for each individual accession), for a total of 430 plants (43 accessions × five control × five droughted plants). Both control and drought treatment were well-watered for the first 28 days, maintaining the soil relative water content at field capacity as measured by monitoring pot weight daily and adding water when necessary. After 28 days, soil in the drought treatment was allowed to dry down. These pots were then rewatered to soil saturation once every 10 days for a total of 14 drought cycles until the conclusion of the experiment 175 days after seeds were sown. Here, as in the natural environments we sought to mimic, the soil water content was not adjusted based on the size of individual plants. Our protocol simulated the natural recurring cycle of rainfall and drought. Such cycles are often used in studies of natural variation (i.e. Exposito-Alonso *et al.*, 2018b; Exposito-Alonso *et al.*, 2019) and in field trials on crop cultivars (IRRI, 2021). In contrast, the well-watered treatment was maintained near field capacity throughout the experiment. Plants were spatially randomized within the greenhouse every week throughout the experiment. At the end of the experiment, nine accessions within the drought treatment with mortality rates higher than 40% (i.e., at least two of the five replicates; Table P1) were excluded from downstream analyses.

Photographs of the rosettes were taken at the time of flowering and subsequently analyzed using ImageJ (http://imagej.nih.gov/ij/) to determine the projected leaf area for each accession under both well-watered and drought treatments (Fig. S1; Table P1).

Determination of relative leaf area and plasticity

Relative leaf area (rLA) is defined here as the leaf area (LA) at the time of flowering for each accession under each experimental condition (either well-watered or drought) relative to all the accessions under the same condition. The relative leaf area of a given accession under well-watered conditions ($rLA_{i\ (well\text{-}watered)}$) is thus calculated as:

$$rLA_{i\ (well-watered)} = \frac{LA_{i\ (well-watered)}}{LA_{m\ (well-watered)}}$$

where $LA_{i\ (well\text{-}watered)}$ is the leaf area of any individual accession, and $LA_{m\ (well\text{-}watered)}$ is the average leaf area for all accessions grown under the same conditions. Similarly, the relative leaf area under drought ($rLA_{i\ (drought)}$) for each accession is calculated as:

$$rLA_{i\ (drought)} = \frac{LA_{i\ (drought)}}{LA_{m\ (drought)}}$$

where $LA_{i\ (drought)}$ is the leaf area of any individual accession under drought and $LA_{m\ (drought)}$ is the average value for all accessions when grown under drought. A high rLA reflects greater vegetative growth of any given accession relative to the set of accessions utilized in this study. The use of rLA, rather than actual values, was essential to allow a normalized comparison of the leaf area of each accession between the watering regimes. Reaction norms based on rLA were employed to quantify plastic changes in relative leaf area between the two treatments (well-watered vs. drought). Leaf area plasticity indexes were calculated based on an established definition (Weijschedé *et al.*, 2006). The leaf area plasticity index to drought (PI) was calculated for each accession as follows:

$$PI = rLA_{i\ (drought)} - rLA_{i\ (well-watered)}$$

A positive leaf area plasticity index does not necessarily imply that the leaf area for that accession was higher under drought, but rather that under drought, a given accession displays a higher rLA relative to the rest of accessions in the study.

Genome-wide association study

Genome-Wide Association Studies (GWAS) identify genetic variants associated with natural variation in a phenotypic trait of interest. We used a GWAS approach to identify polymorphisms associated with natural variation in rLA and its plasticity. The online tool GWAPP (http://gwas.gmi.oeaw.ac.at/) was employed using a linear regression model (Seren *et al.*, 2012). The linear regression model does not address the confounding effects of population stratification, family

144 structure, and cryptic relatedness (Price *et al.*, 2010); however, these issues are minimized by our
145 choice of a regional (Iberian) population (Frachon *et al.*, 2018; Tabas-Madrid *et al.*, 2018; Frachon
146 *et al.*, 2019). Nonetheless, we demonstrate that the candidate SNPs discussed here were also
147 significant after the application of a mixed model approach implemented either using GWAPP (Seren
148 *et al.*, 2012) or GWAS-Flow (Freudenthal *et al*., 2019) (Figs S2, S3, and S4; Tables G1-G6),
149 providing further confidence in our results.

150 We filtered out low-frequency variants (minor allele frequency (MAF) < 10%) to focus on
151 variants less likely to be undergoing negative selection or to be spurious SNPs from sequencing
152 errors. We obtained gene model annotation from the TAIR11 genome release. We defined the
153 'consensus' transcript variant as the variant producing the longest transcript. We predicted the effect
154 of every SNP using SnpEff (Cingolani *et al.*, 2012). We focused on SNPs within gene transcriptional
155 units, including introns, untranslated regions at the 5′ and 3′ ends, and open reading frames, as defined
156 in Araport11 (Cheng *et al.*, 2017). We also included the promoter region, defined as 5 kb upstream
157 of the most distal transcription start site. We imposed a stringent arbitrary significance threshold
158 corresponding to a score of four ($P < 0.0001$; Fig. S5A-E).

159 Using the results from GWAS obtained from the association with rLA, we obtained reaction
160 norms that reflect plastic or homeostatic patterns of genome-wide associations of these traits in
161 response to drought. The association between a phenotype and any given SNP was designated as
162 homeostatic if it was found significantly associated with that trait under both conditions (well-watered
163 and drought).

164

165 **Transcriptome-wide association**

166 Natural variation in gene expression is an important mechanism of local adaptation (Des Marais *et*
167 *al.*, 2012; Lasky *et al.,* 2014). Transcriptome-Wide Association Studies (TWAS) identify variation
168 in transcript abundance associated with observed variation in phenotypic traits (Gusev *et al.*, 2016;
169 Kremling *et al.*, 2019). TWAS analysis does not suffer from the limitations imposed by false non-
170 causal synthetic associations due to linkage disequilibrium (Li *et al.*, 2021) that are typical of GWAS
171 (Korte and Farlow 2013). Also, TWAS evaluates continuous variation in transcript abundance rather
172 than the discrete presence/absence of SNPs with (potentially) additive or synergistic effects on a
173 continuous phenotype. We retrieved the transcriptome data from rosette leaves of 727 Arabidopsis
174 accessions from the GEO dataset with accession number GSE80744 and SRA study SRP074107

175 (Kawakatsu *et al.*, 2016) and subsetted the 35 Iberian accessions that overlapped with the 43 Iberian
176 accessions used in our study. Data wrangling was conducted utilizing the dplyr (Wickham *et al.*,
177 2015) and tidyr (Wickham and Henry, 2018) packages. Spearman's rank correlation coefficients
178 between the variation in individual phenotypic values (relative leaf area (rLA_i), plasticity index (PI),
179 and intrinsic water use efficiency (WUE_i) from Dittberner *et al.* (2018; Tables P1 and P2)), and
180 individual transcript abundance values within the study population, were calculated using the
181 correlation function of the Hmisc package (Harrell Jr and Dupont, 2019). The stronger the association
182 of the two variables, the closer the Pearson's correlation coefficient, r_s, will be to either +1 or -1. We
183 imposed a threshold based on this correlation coefficient ($|r_s| \geq 4.0$). We considered this threshold to
184 be stringent after inspection of the distribution of the results (Fig. S5F-J). We include the r_s and
185 corresponding *P*-values in Tables T1 and T2.
186 Using the results from TWAS, we derived reaction norms to reflect homeostatic patterns of
187 transcriptome-wide associations of rLA in response to drought. Any given transcript was designated
188 homeostatic if found significantly associated with rLA (either positively or negatively; $|r_s| \geq 4.0$)
189 under both conditions (well-watered and drought).
190

191 **eGWAS**

192 Natural variation in transcript abundance can also be used to identify candidate SNPs (expression
193 SNPs or eSNPs) that control transcript abundance in an Expression Genome-Wide Association Study
194 (eGWAS). eGWAS was conducted by compiling the transcript abundance values of a given gene of
195 interest, extracting the transcript abundance for that particular gene in the 727 Arabidopsis accessions
196 from the GEO dataset with accession number GSE80744 and SRA study SRP074107 (Kawakatsu *et*
197 *al.*, 2016), then subsetting the 665 accessions included in the 1001 Genomes project (The 1001
198 Genomes Consortium, 2016). Then, the online tool GWAPP (http://gwas.gmi.oeaw.ac.at/) was
199 employed using a linear regression model (Seren *et al.*, 2012) to identify candidate regulatory
200 variants. Regulatory variants are either cis- or trans-acting, depending on the location of the genetic
201 variant. cis-eSNPs were defined as those located within the ORF, introns, UTRs, or the promoter
202 region of the regulated gene. Trans-eSNPs were defined as those located within the ORF, introns,
203 UTRs, or promoter region of a gene different from the gene transcriptionally regulated by that genetic
204 variant.

Analyses

AraCLIM (https://github.com/CLIMtools/) is a database that describes the local environment of the Arabidopsis accessions sequenced as part of the 1001 Genomes Project (Ferrero-Serrano and Assmann, 2019; Ferrero-Serrano et al., 2022). We obtained from AraCLIM the values for MOD17A2 (Net Primary Productivity in the spring season) (Heinsch *et al.*, 2003; Running and Zhao, 2015) at the collection site of each accession and evaluated the correlation with the phenotypes obtained in our experiment.

WUE_i is defined as the ratio between instantaneous carbon gain and transpirational water loss, typically calculated per unit of leaf area (Condon *et al.*, 2002). To integrate information from previously published studies on the Iberian Arabidopsis population, we retrieved available data on natural variation in intrinsic water use efficiency (WUE_i, $\delta^{13}C$), previously recorded by Dittberner *et al.* (2018). During photosynthesis, plants discriminate against $^{13}CO_2$ in the reaction center of *Ribulose 1, 5-biphosphate carboxylase/oxidase* (*RuBisCO*). As stomata close, minimizing water loss in response to drought, the discrimination against $^{13}CO_2$ decreases because the internal CO_2 concentration (C_i) becomes unavoidably reduced. As a result of their reduced C_i, plants with greater WUE_i experience lower CO_2 concentrations at the sites of carboxylation (C_c) and have less negative $\delta^{13}C$ values.

All statistical analyses and figures were produced using R (Team, 2013). The code and data to reproduce the analysis, figures, and tables are available at https://github.com/AssmannLab and Zenodo. Gene Ontology (GO) biological process analysis (Tables GO1-GO10) was performed using the open-source software ShinyGO v0.61: http://bioinformatics.sdstate.edu/go60/ (Ge *et al.*, 2020) with the following settings: the search species was "*Arabidopsis thaliana*," the *P*-value cutoff (FDR) was 0.05, and the number of most significant terms to show was ten. To replicate these results, the lists of genes that were input into these analyses based on significance thresholds can be selected from Tables G1-G6, T1, and T2. Each analytical technique used in this study has assumptions and limitations, which we discuss in Document S1. The code and data necessary to reproduce all analyses and figures in this study are available on GitHub (https://github.com/AssmannLab).

232 **Results**

233 **Natural variation in leaf area and plasticity in response to long-term cyclical**
234 **drought**

235 To quantify phenotypic variation in Iberian Arabidopsis accessions exposed to drought, we conducted
236 a common garden experiment (Fig. 2A). We used image analysis to derive rosette leaf area under
237 well-watered or drought conditions (Figs 2B, S1; Table P1). As expected, we observed a significant
238 ($P < 0.001$) reduction in leaf area resulting from drought in most genotypes, as evidenced by the
239 phenotypic reaction norms. In contrast, a small number of accessions exhibited constant or increased
240 leaf area under drought (Fig. 2B; Table P1), demonstrating that a reduction in leaf area in drought is
241 not inescapable. Based on these data, we calculated the relative leaf area (rLA) of each accession
242 under both well-watered and drought conditions (see Materials & Methods; Fig. 2C; Table P1). We
243 used rLA rather than the actual leaf area to allow comparison of the leaf area of each accession relative
244 to the study population for each watering regime. We also show that the plasticity index derived from
245 the difference in rLA between conditions (i.e. reflecting the slopes of the reaction norms in Fig. 2C;
246 Table P1) is proportional to the fold change in leaf area under drought relative to well-watered
247 conditions (Fig. S6).

248 We explored the relationship between rLA in the absence of drought and its plastic response
249 (plasticity index; PI) to drought. Fig. 2D shows that accessions with higher rLA under well-watered
250 conditions displayed greater plastic reductions in rLA when subjected to drought (negative leaf area
251 plasticity; yellow datapoints in Figs 2D, E). On the contrary, accessions with lower rLA under well-
252 watered conditions displayed homeostatic phenotypic responses to drought (Fig. 2D, E blue
253 datapoints). Despite this overall trend, we also observed individual accessions with high rLA under
254 well-watered conditions and positive plasticity indexes under drought (green datapoints in Fig. 2D
255 and Fig. 2E). Conversely, a few accessions displayed low rLA and negative leaf area plasticity
256 indexes (red datapoints in Fig. 2D and Fig. 2E).

257 While the severity of drought depends on multiple environmental parameters, its
258 physiological response is very characteristic. It results in stomatal closure and a reduction in CO_2
259 assimilation, as reflected in decreases in Net Primary Productivity (NPP), an index that, therefore,
260 can be used as a reliable drought indicator (Huang *et al.*, 2016). We determined that the plastic leaf
261 area responses (negative values of leaf area plasticity index) we observed in our study were typical

262 of accessions from more productive habitats as reflected in Net Primary Productivity in spring (NPP
263 spring; Fig. 3A). In contrast, homeostatic leaf area responses (zero or positive values of leaf area
264 plasticity index) were typical of accessions from less productive habitats (Fig. 3A).

265 Genetic variants significantly associated with leaf area plasticity were identified by GWAS
266 (Fig. 3B; Table G3). Gene ontology (GO) analysis of functions associated with the genes harboring
267 the variants identified by GWAS revealed an enrichment in auxin-related processes (Table GO1).
268 Among the variants identified from GWAS (Fig. 3B; Table G3) as associated with leaf area plasticity,
269 we highlight two co-varying SNPs in the 5' and 3' UTR that comprise a haplotype of *SMALL AUXIN*
270 *UP RNA 26* (*SAUR26***,** AT3G03850) (Fig. 3C). These variants were identified by GWA analysis using
271 a linear model (Fig. 3B; Table G3). To confirm that the identification of these candidates was not an
272 artifact due to population structure, we verified that these variants were also identified using two
273 different analyses that correct for population structure in the sample: an Accelerated Mixed Model
274 using GWAPP and an alternative Mixed Model approach, GWAS-Flow (these two SNPs are among
275 the green datapoints in Fig. S7A and C; see Table G3).

276 We additionally found from TWA analysis that the transcript levels of *SAUR26* are also
277 correlated with natural variation in leaf area plasticity in response to drought (Tables T1, T2).
278 eGWAS confirmed the cis-regulatory effect of the same two genetic variants as depicted in Fig. 3C
279 (cis-regulation; Fig. 3D; Table G6), consistent with the correlation between the genetic variation in
280 *SAUR26*, its transcript abundance, and leaf area plasticity.

281 Fig. 3E illustrates the haplotypic differences in leaf area plasticity for *SAUR26* in our study.
282 Accessions harboring the minor *SAUR26* haplotype display negative plasticity in rLA, while the
283 major *SAUR26* haplotype is associated with homeostatic and positive plasticity responses in rLA (Fig.
284 3E; Wilcoxon P-value < 0.001). These haplotypic differences were also associated with the transcript
285 levels of *SAUR26* (Fig. 3F), which we confirmed not only in the group of accessions included in our
286 study (Wilcoxon P-value < 0.001) but also in the much larger group of 189 Iberian accessions
287 included within the 1001 Genomes Project (Fig. 3F; Wilcoxon P-value < 0.001). Both the genetic
288 variation defined by this haplotype in *SAUR26* and the resulting *SAUR26* transcript abundance are
289 associated with the interplay between plasticity and homeostasis that we determine in our study (Figs
290 3E, F). These results highlight *SAUR26* as a candidate regulator of leaf area plasticity in response to
291 drought (Figs 3G, H).

292 In our GWA analysis on rLA (Fig. S8A, Table G1, G2), no SNPs were associated with rLA
293 under both well-watered and drought conditions, i.e., no SNPs were associated with homeostasis and
294 thus horizontal lines are absent from Fig. S8A. The results from TWA analysis were strikingly
295 different, identifying not only transcripts associated with leaf area plasticity but also transcripts
296 associated with leaf area homeostasis (Fig. 4; Fig. S8B). Regarding homeostasis, four transcripts are
297 positively correlated with rLA under both well-watered and drought conditions: *SOFL2*
298 *(AT1G68870), CPN60B (AT1G55490), AT5G39471, and CKL8 (AT5G43320)* (Fig. 4A). Accessions
299 with higher transcript abundance of these genes display a higher rLA under both well-watered and
300 drought conditions (Fig. 4B-E; note the similarity of the regression lines in each panel). Conversely,
301 we identified four genes negatively correlated with rLA: *RHF1A* (AT4G14220), *AT5G60160*,
302 *AT4G15260*, and *AT5G16800* (Fig. 4F). Accessions with a higher transcript abundance of these genes
303 display lower rLA under both well-watered and drought conditions (Fig. 4G-J; note the similarity of
304 the regression lines in each panel).
305

306 **Trade-off between plasticity and intrinsic water use efficiency**

307 It was not surprising to find a trade-off between growth and drought resistance among the accessions
308 in our study (Fig. 2D), as this is a well-established phenomenon (Zhang *et al.*, 2020). Accordingly,
309 we hypothesized that those accessions that displayed a homeostatic response to drought minimized
310 water loss, and thus would exhibit an increased intrinsic water-use efficiency (WUE_i). Given that
311 $\delta^{13}C$ reflects intrinsic water use efficiency (WUE_i) (Juenger *et al.*, 2005; Easlon *et al.*, 2014), we
312 analyzed the $\delta^{13}C$ values recorded by Dittberner *et al.* (2018), available for 21 of the accessions used
313 in our study. The results confirm a trade-off between plasticity and WUE_i (Fig. 5A). Accessions that
314 exhibit strong negative plasticity following drought (negative leaf area plasticity indices) have a lower
315 WUE_i in the absence of drought (more negative $\delta^{13}C$ values). Those accessions that maintain or
316 increase leaf area in response to drought (positive leaf area plasticity indices) display a higher WUE_i
317 in the absence of drought (more positive $\delta^{13}C$ values).
318 GWA analysis failed to identify any genetic variants associated with the observed phenotypic
319 trade-off between intrinsic WUE_i and leaf area plasticity (Fig. 5B; Table G3, G4), i.e., no datapoints
320 in the upper right quadrant of Fig. 5B. However, TWA analysis (Fig. 5C) provided insight into this
321 trade-off. Red datapoints in Fig. 5C are transcripts with greater abundance in those negatively plastic
322 and less water-use efficient accessions depicted in red in Fig. 5A; GO analysis revealed that these

323 were enriched in processes involved in RNA modification (Table GO2); we chose the putative
324 pseudouridine synthase *CBF5* (*AT3G57150*) as an example (Figs 5D, E). Conversely, green points in
325 Fig. 5C represent transcripts with greater abundance in the homeostatic and water-use efficient
326 accessions depicted in green in Fig. 2D. We chose *CYCLIC NUCLEOTIDE-GATED CHANNEL 16*
327 (*AT3G48010*; *CNGC16*) as an example (Figs 5F, G).
328 We determined that in our study, accessions that in response to drought displayed either
329 increased or homeostatic leaf area plasticity also had higher WUE_i in the absence of drought (Fig.
330 5A). We then conducted a meta-analysis on the 95 Iberian accessions with published $\delta^{13}C$ information
331 (Dittberner *et al.*, 2018). GWA analysis of these accessions rendered a distinctive peak in a single
332 gene, identifying a haplotype consisting of eight co-varying SNPs in *ClpX3* (*AT1G33360*; Fig. 6A;
333 Table G5), an ATP-dependent Clp protease subunit that plays essential roles in chloroplast
334 development (Kim *et al*., 2009). Consistent with this result but more informative was the TWA
335 analysis of WUE_i in the 88 Iberian accessions with both published transcript abundance and $\delta^{13}C$
336 information (Fig. 6B): we uncovered a distinctive enrichment in photosynthesis-related genes (Fig.
337 6C; Table GO3) among transcripts that are upregulated in accessions with high WUE_i (more positive
338 $\delta^{13}C$ values; Fig. 6B; Table T1, T2). We highlight the positive relationships with WUE_i uncovered
339 for the transcript abundance of *RuBisCO small subunit 2B* (*AT5G38420*; *RBCS2B;* Fig. 6D) and the
340 positive relationship between the transcript abundance of *SAUR26* and WUE_i (Fig. 6E), in
341 concordance with other findings in our study.
342

343 # DISCUSSION

344

345 ## Identifying candidate regulators of plasticity and homeostasis

346 An adaptive trade-off between growth and drought resistance in plants is well-established (Zhang *et*
347 *al.*, 2020). In productive environments, accessions with higher rLA in the absence of drought may
348 have an advantage in competing for aboveground resources relative to smaller individuals, as
349 proposed by Tilman (1988). On the other hand, plants adapted to unproductive environments typically
350 fix less carbon, have higher WUE_i, and display reduced vegetative growth, even when grown in rich
351 environments (Parsons, 1968; Chapin, 1991); however, these plants are typically stress-tolerant
352 (Billings and Mooney, 1968; Grime, 1974, 1977). In our study, accessions typical of more productive
353 areas display strong and negative plastic responses to drought (Fig. 3A). Conversely, accessions with

354 homeostatic or even positive plasticity in rLA in response to drought typify less productive areas (Fig.
355 3A). Here, we sought to identify the genetic basis of these contrasting ecological strategies.
356 Our main interest was not to identify natural variation associated with well-watered or drought
357 phenotypes, but rather natural variation associated with the degree of plasticity evoked in response to
358 drought, i.e., natural variation associated with reaction norms, rather than with phenotypes in one
359 environment or the other (well-watered or droughted). In exploring the genetic basis of plasticity, we
360 identified 31 genes corresponding to the top 50 candidate SNPs with the strongest association with
361 the leaf area plasticity index (Fig. 3B; Table 1; Table G3). To the best of our knowledge, 20 out of
362 these 31 genes have been previously characterized, and many of these are related to auxin regulation
363 and leaf expansion. This enrichment in auxin-related processes was confirmed by GO analysis (Table
364 GO1). Notably, when we compare the candidates resulting from GWA analysis on rLA vs. leaf area
365 plasticity, only eight candidate SNPs overlapped between both traits (green datapoints in Fig. S9A),
366 and none of these eight SNPs are in genes related to auxin. In other words, the auxin-related candidate
367 genes are related to *plasticity* in this trait and not to the trait itself.
368 The variant with the strongest association with the plastic response to drought was the auxin
369 efflux carrier family protein *PIN8* (*AT5G15100*). Among the associated SNPs, we also found two co-
370 varying SNPs in *AUXIN RESPONSE FACTOR 16* (*ARF16*; *AT4G30080),* two co-varying SNPs in
371 *SMALL AUXIN UP RNA 26* (*SAUR26*; *AT3G03850*); two variants in *AGAMOUS-like 15*
372 (*AT5G13790*; *AGL15*), a gene that negatively regulates auxin signaling in Arabidopsis (Zheng *et al.*,
373 2016); and three variants in *LONESOME HIGHWAY LIKE 1* (*LL2*; *AT2G31280*), an atypical basic
374 helix-loop-helix (bHLH) transcription factor that regulates early xylem development downstream of
375 auxin (Ohashi-Ito *et al.*, 2013).
376 Among the candidates that are not formally included in the GO category "response to auxin,"
377 we found six co-varying SNPs in the abscisic acid receptors *PYR1-like 11* (*PYL11*; *AT5G45860*) and
378 *PYR1-like 12* (*PYL12*; *AT5G45870*). ABA and auxin pathways interact in the regulation of growth
379 (Emenecker & Strader 2020), and also in the regulation of plasma membrane H^+ ATPases (of which
380 there is one member in the list, *H^+ ATPase 2* (*AHA2; AT4G30190*)) during cell expansion (Spartz *et*
381 *al.,* 2014) and stomatal control (Wong *et al*., 2021). We also found four co-varying SNPs in the *Basic*
382 *helix-loop-helix (bHLH) DNA-binding family protein MYC3* (*AT5G46760*), a known regulator of
383 glucosinolate biosynthesis (Schweizer *et al.*, 2013). Auxin negatively regulates glucosinolate levels,
384 which appears to integrate growth and stomatal regulation during drought (Salehin *et al.*, 2019) and

385 ABA response (Zhao *et al*., 2008). GO biological process analysis on positively correlated candidates
386 resulting from TWAS analysis on leaf area plasticity index for drought also revealed an enrichment
387 of glucosinolate biosynthesis genes (Table GO4).

388 We found that among the auxin-related variants associated with leaf area plasticity (Fig. 3B),
389 SNPs in *SAUR26* were of particular interest. The majority of characterized *SAUR* genes are positive
390 regulators of plant growth (Spartz *et al.*, 2014; Li *et al.*, 2015; Stortenbeker and Bemer, 2019). The
391 two associated variants in *SAUR26* were found in the 5' and 3' UTR, respectively (Fig. 3C), regions
392 of the transcript that typically regulate gene expression. Indeed, we found the transcript levels of
393 *SAUR26* to be associated with this genetic variation in *SAUR26* itself (cis-regulation; Fig. 3D), which
394 we confirmed both in the group of accessions included in this study and, importantly, in the larger
395 group of 189 Iberian accessions in the 1001 Genomes Project (Fig. 3F). The minor haplotype is
396 associated with negative plasticity in leaf area in response to drought. Conversely, the major
397 haplotype, associated with higher transcript abundance of *SAUR26*, is associated with leaf area
398 homeostasis and positive plastic responses (Fig. 3E).

399 Natural variation in transcript abundance of *SAUR26* explained 18% of the observed plastic
400 response in leaf area to drought in our study (Fig. 3G, H). The importance of *SAUR26* is supported
401 by previous work that revealed natural genetic variation in *SAUR26* associated with growth thermo-
402 responsiveness of the rosette compactness index (Wang *et al.*, 2019), and cis-elements in the 5'
403 upstream region or the 3'UTR region of *SAUR26* that were responsible for this response (Wang *et al.*
404 2021). This conclusion is also supported by our meta-analysis of the larger Iberian population with
405 transcriptome data, which also identified *SAUR26* transcript abundance as positively correlated with
406 higher WUE_i (Fig. 6B, E), along with other related auxin-related transcripts such as *AUXIN*
407 *RESISTANT 3* (*AXR3*, also known as *IAA17*, *AT1G04250;* Fig. S10A) (Leyser *et al.*, 1996) and
408 *SMALL AUXIN UPREGULATED 15* (*SAUR15*, *AT4G38850*; Fig. S10B) (Oh *et al.*, 2014). As we
409 uncover in this study, both transcript abundance and natural genetic variation in *SAUR26* cis-
410 regulatory elements are associated with the interplay between plasticity and homeostasis in rLA
411 following drought stress (Fig. 3, Tables G3, T1, T2).

412 Interestingly, the minor haplotype frequency for this *SAUR26* haplotypic variant in our study
413 sample (minor haplotypic frequency, MHF = 38.09%) is similar to the frequencies we find in the 189
414 accessions within the Iberian population (MHF = 35.98%). However, the minor haplotype in the
415 Iberian population becomes the haplotype in higher frequency (64.14%) in the global 1001 Genomes

416 collection (The 1001 Genomes Consortium, 2016). It has been shown that Iberian Arabidopsis
417 populations locally adapted to drought conditions in this region out-perform accessions from wetter
418 areas of Northern Europe when both are exposed to drought (Exposito-Alonso *et al.*, 2019).
419 Following this, given that the major haplotype in our study is associated with homeostatic responses
420 to drought (Fig. 3E) and that its frequency becomes reduced outside the drought-prone Iberian region,
421 we can speculate that this *SAUR26* haplotypic variant is under selection in the Iberian population,
422 conferring an adaptive advantage to the water-limited conditions of the region.

423 We did not identify any SNPs associated with rLA under both well-watered and drought
424 conditions. Therefore, the genetic basis of growth homeostasis under drought could not be defined in
425 our study using GWAS (Fig. S8A). On the other hand, the reaction norms based on the strength of
426 association of transcript abundance with rLA, i.e., TWAS, identify four transcripts that are positively
427 correlated with rLA under both well-watered and drought conditions (Figs 4A-E, S8B). This means
428 that accessions with greater transcript abundance for those genes display higher rLA under both well-
429 watered and drought conditions. Conversely, we identified four transcripts negatively correlated with
430 rLA such that accessions with a higher transcript abundance of those genes display lower rLA under
431 both well-watered and drought conditions (Fig. 4F-J). Therefore, these eight genes are strong
432 functional candidates for the homeostatic regulation of rLA.

433 Of the eight resultant candidate genes, *CPN60B* (homeostatic, higher rLA) encodes a rubisco
434 large subunit-binding protein (Cheng *et al.*, 2020). *SOFL2* (homeostatic, higher rLA) is implicated in
435 the control of cytokinin content (Zhang *et al*., 2009), which can contribute to drought tolerance
436 (Rivero *et al.*, 2007), while *AT4G15260* (homeostatic, lower rLA) is a putative UDP-
437 glycosyltransferase, with another member of this superfamily identified as a cytokinin
438 glycosyltransferase (Hou *et al.*, 2004) that improves vegetative-stage drought survival when
439 overexpressed. *AT5G16800* encodes a N-terminal acetyl transferase for which null mutants exhibit
440 sensitivity to salinity stress. We can surmise functions in homeostatic control of leaf area for these
441 four genes based on their described functions and phenotypes. The other four homeostatic genes are
442 *AT5G39471* (annotated as a "Cysteine/Histidine-rich C1 domain family protein") and *CKL8*
443 (annotated as a casein kinase), both correlated with homeostatic and high rLAs, and *RHF1A* (RING-
444 finger E3 ubiquitin ligase (Liu *et al.*, 2008) and *AT5G60180* (vacuolar aminopeptidase (Park *et al.*,
445 2017), both correlated with homeostatic and low rLAs. For these genes further research is needed
446 regarding how they might contribute to homeostasis.

447

448 **Trade-off between relative leaf area (rLA), plasticity and WUE_i**

449 Plant species with low relative growth rates exhibit high WUE_i (Angert *et al.*, 2009; Kimball *et al.*,
450 2012). We can hypothesize that those plants with lower growth rates will have better drought
451 resistance, consequently displaying growth homeostasis. These observations are both consistent with
452 results from ecological studies and confirmed in crop species (Kasuga *et al.*, 1999; Ferrero-Serrano
453 and Assmann, 2016; Ferrero-Serrano *et al.*, 2018; Ferrero-Serrano et al., 2024). In our study,
454 accessions with lower rLA and homeostatic responses to drought display a greater abundance of
455 transcripts encoding functions related to ion transport (yellow datapoints in Fig. S9B; Tables T1, T2,
456 GO5), which could be related to osmoregulation and stomatal control of transpiration. Consistent
457 with this argument, the homeostatic response in rLA in response to prolonged drought that we observe
458 in our study correlates positively with a high predicted WUE_i recorded by Dittberner *et al.* (2018) for
459 the same accessions (Fig. 5A).

460 We then studied the genetic basis of this trade-off between rLA, plasticity, and WUE_i. There
461 were no SNPs associated with both the leaf area plasticity index and WUE_i (Fig. 5B). However, when
462 we compare the candidates obtained from TWA analysis, we identify transcripts associated with both
463 low WUE_i and a negative plastic response in leaf area following sustained drought (Fig. 5C).
464 Conversely, we also identify a set of transcripts that is significantly associated with both leaf area
465 homeostasis (more positive leaf area plasticity index) and increased WUE_i (Fig. 5C). To exemplify
466 these opposed responses to drought, given the enrichment in RNA modification and ion transport
467 genes that we found in the transcripts regulating the trade-off between relative leaf area and plasticity
468 (Fig S12B; Tables T1, T2), we highlight two of the genes identified by TWAS, with opposite
469 correlations between transcript abundance and relative leaf area plasticity (Figs 5D, E vs. Figs 5F,
470 G): (*CBF5*; *AT3G57150*) and *CYCLIC NUCLEOTIDE GATED CHANNEL 16* (*CNGC16*;
471 *AT3G48010*).

472 *CBF5* encodes a protein with homology to a category of pseudouridine synthases, and its
473 knockout in Arabidopsis is lethal (Lemontova *et al.,* 2007). Originally only non-coding RNAs,
474 particularly rRNAs, were thought to be pseudouridylated, but it is now recognized that mRNAs are
475 also a target for pseudouridylation. In both yeast and human cells, this post-transcriptional
476 modification is induced by heat shock, with consequent impacts on splicing, mRNA stability, and
477 translation (Karijolich *et al*., 2015), and some candidate pseudouridine synthases in rice have been

478 shown to be transcriptionally regulated by drought (Dingra et al., 2023). We observe that accessions
479 with higher transcript abundance of *CBF5* display both strong negative plastic responses in rLA in
480 response to drought (Fig. 5D) and reduced WUE_i (Fig. 5E). Our observations suggest that stress-
481 induced pseudouridylation may also occur in plants, with functional consequences for drought
482 tolerance; other types of mRNA modifications in plants have been correlated with increased mRNA
483 stability and translation under salinity stress (Kramer et al., 2020) and improved heat tolerance (Tang
484 *et al.,* 2020).

485 Conversely, transcript abundance of *CNGC16* is associated with homeostatic responses in
486 rLA and increased WUE_i. CNGCs are a superfamily of ion channels permeable to divalent and
487 monovalent cations (Köhler *et al.*, 1999; DeFalco *et al.*, 2016). *CNGC*s like *CNGC5* and *CNGC6*
488 have been reported to be the basis of a cyclic GMP (cGMP)-activated nonselective Ca^{2+}-permeable
489 cation channel activity in the plasma membrane of Arabidopsis guard cells (Wang *et al.*, 2013)
490 associated with stomatal closure. *CNGC16* is also critical for reproductive success following drought
491 stress (Tunc-Ozdemir *et al.*, 2013). Consistent with these functional roles, in our study, higher
492 transcript abundance of *CNGC16* is found in accessions with positive leaf area plasticity indexes
493 under drought (leaf area homeostasis; Fig. 5F); and with high WUE_i (Fig. 5G).

494 Given the increased plastic responses in leaf area found in accessions with lower WUE_i, we
495 next conducted a meta-analysis on the larger set of 95 Iberian accessions with $\delta^{13}C$ information from
496 a previous study focused on the global Arabidopsis population (Dittberner *et al.*, 2018). We identified
497 a distinctive peak consisting of eight co-varying SNPs in a single gene, *ClpX3* (*AT1G33360*; Fig.
498 6A), an ATP-dependent Clp protease subunit (Nishimura and van Wijk, 2015). Null mutants in a
499 different chloroplast protease subunit, ClpR, display a remarkable loss of chlorophyll (95 to 98%
500 reduction) and photosynthetic capacity, turning entirely white when grown under high light (Kim *et*
501 *al.*, 2009).

502 TWA analysis of WUE_i determined from $\delta^{13}C$ values in the 88 Iberian accessions with both
503 $\delta^{13}C$ information (Dittberner *et al.*, 2018) and published transcript abundance (Kawakatsu *et al.*,
504 2016) further supported the relationship with photosynthesis. Our TWAS on WUE_i in the larger
505 Iberian population identified 31 out of the 45 candidate genes for WUE_i that we also identified in the
506 subset of 20 Iberian accessions in our experimental study for which published $\delta^{13}C$ data were
507 available (Table T1 and T2). Gene Ontology (GO) biological process analysis of the resultant 45
508 candidates positively correlated with $\delta^{13}C$ uncovered an unequivocal enrichment in photosynthesis-

509 related genes for transcripts that are upregulated in accessions with high WUE_i (less negative $\delta^{13}C$
510 values; Figs 6B, 6C; Table GO3). Among the candidates from our TWA analysis that are positively
511 related to WUE_i was *RuBisCO small subunit 2B* (*AT5G38420*; *RBCS2B;* Figs 6B, D). An
512 upregulation in *RuBisCO* may compensate for suboptimal CO_2 concentrations at the sites of
513 carboxylation arising from reduced stomatal apertures in plants from drought-prone environments.
514 We illustrate eight additional genes with transcript abundances that were positively associated with
515 WUE_i in Fig. S10. Among these are *NADH dehydrogenase-like complex M* (*NdhM*, *AT4G37925;* Fig.
516 S10C), required for *NdH* complex assembly (Ifuku *et al.*, 2011), and *High cyclic electron flow 1*
517 (*HCEF1*; *AT3G54050*; Fig. S10D; Livingston *et al.*, 2010), both regulators of cyclic electron flow
518 around PSI (Yamori *et al.*, 2011), *ATP-Synthase δ-Subunit* (*ATPD*, *AT4G09650*; Fig. S10E)
519 (Maiwald *et al.*, 2003), *Photosystem I reaction center subunit PSI-N* (*PSAN*, *AT5G64040;* Fig. S10F)
520 (Haldrup *et al.*, 1999), and *Photosystem II subunit O-2* (*PSBO2*; *AT3G50820;* Fig. S10G) (Murakami
521 *et al.*, 2005). Also, the candidate with the highest association score is a member of the plasma
522 membrane intrinsic protein (PIP) subfamily of aquaporins (*PIP1;5*; *AT4G23400*; Fig. S10H). PIPs
523 regulate water flux in guard cells as well as membrane permeability to CO_2 in the mesophyll, with an
524 important effect on mesophyll conductance and CO_2 concentration at the sites of carboxylation (C_c)
525 (Groszmann *et al.*, 2017; Zait, Ferrero-Serrano & Assmann 2021). Thus, *PIP1;5* is also a candidate
526 regulator of photosynthetic rates. As discussed before, *SAUR26* is also among these candidates (Fig.
527 6B, E), increasing our confidence in the role of this gene as a regulator of plastic responses to drought
528 (Fig. 3).

529 Among the candidates that are negatively related to high WUE_i there is an enrichment in
530 carbohydrate transport-related processes (Table GO6). We can speculate that this enrichment reflects
531 the transport of carbohydrates produced during photosynthesis to promote plant growth. This would
532 be concordant with the trade-off between growth and WUE_i that we observe in our study.
533

534 **Conclusions**

535 The adaptive role of plasticity has been at the center of a long-standing debate. Much work and
536 discussion have focused on the principle that if plasticity is indeed adaptive, it may be under genetic
537 control (Bradshaw, 1965; Via *et al.*, 1995); however, few relevant genes have been identified. Here,
538 we propose that not only plasticity but also homeostasis is under genetic control and subject to natural
539 selection. This concept is supported by our dissection of the genetic basis of both plasticity and

540 homeostasis in leaf area following drought, which identifies specific genes implicated in each
541 process.

542 Knowledge from natural populations of how plants adapt to their environment can be
543 incorporated in breeding and biotechnological approaches to crop improvement. In this study, we
544 observe a trade-off between growth and drought response. A similar trade-off between stress
545 tolerance and productivity threatens food security. It is noteworthy that we also found accessions that
546 did not display this trade-off, e.g., those accessions marked in green in Fig. 2D, E. These accessions
547 may be of particular interest from an agronomic perspective.

548 The concerted use of TWAS and GWAS increases the power to link genes to phenotypes
549 (Kremling et al., 2019). A similarly integrative approach has identified water use efficiency traits in
550 sorghum (Ferguson et al., 2020). Here, this approach has yielded insights into the genetic basis of
551 response to resource limitation, identifying both candidate "plasticity genes" and candidate
552 "homeostasis genes" for further study. In particular, the identification of potential homeostatic
553 mechanisms has important implications for maintaining crop yield in the face of climate change.
554 Results arising from diverse genome-wide analyses in both model and crop species (Schindele et al.,
555 2020) can now be used to inform powerful new CRISPR-based approaches for gene editing and
556 modulation of transcript abundance toward crop improvement (Abudayyeh et al., 2017).

557 **Figures**

558 **Fig. 1.** Conceptual framework for the adaptive role of plastic and homeostatic responses across
559 productivity gradients in the local environment. (A) Schematic illustration representing the balance
560 *sensu* Grime (1974, 1977), between stress tolerance in lower productivity, stress-prone environments,
561 and competitive ability in and homeostasis in plants. In less productive environments, homeostatic
562 responses to stress and lower relative growth rates result in lower biomass production, which is tuned
563 in to the lower resources that are typically available in their environment and favors adaptation to
564 those environments. In contrast, in productive environments, in which competition becomes more
565 intense, plastic responses are favored from an adaptive standpoint. (B). In unproductive
566 environments, frequent stress events can increase the allostatic load in individuals adapted to high-
567 productivity environments where plastic responses are beneficial. During the lifetime of an
568 individual, this results in a maladaptive response that increases allostatic load. In contrast, individuals

adapted to unproductive environments exhibit less plastic (more homeostatic) responses to repeated stress that reduces their allostatic load over their lifetime.

Fig. 2. Accession-specific rosette leaf area responses in Arabidopsis. (A) Detail of the common garden experiment, illustrating the randomization of well-watered and drought treatments, as reflected in soil coloration. (B) Phenotypic reaction norms illustrating a reduction of leaf area in response to drought in most but not all accessions. Violin distributions represent probability densities of leaf area (cm^2) among the accessions included in this study. Datapoints depict the mean phenotypic values of individual accessions, and the reaction norms represent the plastic response in the leaf area of each accession in response to drought (t-test; P-value < 0.001). (C) Phenotypic reaction norms illustrating plastic and homeostatic responses in relative leaf area (rLA). Violin distributions represent probability densities of rLA among the accessions included in this study. Datapoints depict the rLA of individual accessions, and the reaction norms represent the plastic response in rLA of each accession in response to drought (t-test; P-value > 0.05). (D) Negative relationship (P-value < 0.05) between leaf area plasticity index (slope of the reaction norms in 2C) in response to drought (y-axis) and rLA under well-watered conditions (x-axis). Data were fitted using a linear regression model. Grey shadow represents the 95% CI of the fit regression line. Four different quadrants are defined by two dashed lines: the average rLA (x-axis), and y = 0, which is the homeostatic point at which a change in water availability does not affect rLA (i.e. a plasticity index of 0). Data points depict individual accessions with their respective label. Data points are colored based on in which quadrant they fall (see text). (E) Images illustrating the plastic and homeostatic responses to drought found among the accessions included in this study.

Fig. 3. *SMALL AUXIN UP RNA 26* (*SAUR26***,** AT3G03850**)** is a candidate regulator of Arabidopsis leaf area plasticity in response to drought. (A) Accessions from more productive areas display stronger negative reductions in leaf area plasticity relative to accessions from less productive environments. Scatter plot depicting the negative relationship (P-value < 0.05) between leaf area plasticity index (y-axis) and Net Primary Productivity during the spring season (x-axis). (B) Manhattan plot representing the strength of association between genetic variants and leaf area plasticity in response to drought. (C) *SAUR26* gene model, including the two co-varying SNPs highlighted in 2B. Orange block depicts the sole exon, green block the 5' UTR, dark green block the 3' UTR. Labels above indicate the position of the two SNPs that co-vary, forming a haplotype in our

600 sample. Major/minor allele frequency in our sample, in the 189 accessions from the Iberian Peninsula
601 included in the 1001 Genome Project, and the whole 1001 Genomes Project sample dataset is
602 provided. (D) Manhattan plot representing the genome-wide strength of association between the
603 genetic variation present within the 665 accessions from the transcript abundance reference panel
604 (Kawakatsu *et al.*, 2016) that overlap with the collection of accessions included in the 1001 Genomes
605 Project, and the variation in the transcript abundance of *SAUR26* (Kawakatsu *et al.*, 2016). The peak
606 in chromosome 3 represents the cis-genetic variants in *SAUR26* affecting its transcript abundance.
607 For the Manhattan plots in 3B and D, the score (y-axis) consists of the negative logarithm of the *P*-
608 value and provides association strength. Each data point represents a SNP with a color corresponding
609 to the chromosome where the genetic variants are located. The x-axis and the different colors shown
610 in the SNPs depicted in the Manhattan plots represent the different chromosomes. The higher the
611 score, the lower the *P*-value, and the stronger the association between genetic variation and leaf area
612 plasticity or *SAUR26* transcript abundance. (E) In the Iberian population, the major haplotype of
613 *SAUR26* is associated with homeostatic or positive responses of relative leaf area (rLA) in response
614 to drought. Conversely, the minor haplotype in the Iberian population is associated with plastic
615 responses in rLA in response to drought. Violin plots show significantly different probability
616 densities of leaf area plasticity in response to drought for the major and minor allele haplotypes in
617 *SAUR26.* (F) The haplotypes in *SAUR26* associated with leaf area plasticity/homeostasis in response
618 to drought are associated with differences in *SAUR26* gene expression. Violin plots show significantly
619 different probability densities of *SAUR26* transcript abundance for the major and minor allele
620 haplotypes in *SAUR26* for both our sample and the entire Iberian population. (G) Scatter plot
621 illustrating the positive relationship between leaf area plasticity index (y-axis) and *SAUR26* transcript
622 abundance (x-axis). For 2A and 2G, the grey shadow represents the 95% CI of the fit regression line
623 (dark grey). (H) Cartoon illustrating the regulatory role of genetic and transcript variation in *SAUR26*
624 and the response of leaf area to drought.

625 **Fig. 4.** Transcriptomic reaction norms uncover genetic correlates of Arabidopsis leaf area
626 homeostasis in response to drought. (A) homeostatic reaction norms for transcripts significantly and
627 positively correlated with relative leaf area (rLA) under both watering regimes. (B) to (E). Scatter
628 plots illustrating positive and homeostatic relationships (*P*-value < 0.05) between rLA under both
629 well-watered (closed circles) and drought conditions (open circles) conditions (y-axis), and transcript
630 abundance (FPKM; x-axis) of (B) AT5G39471, (C) *SOB FIVE-LIKE 2* (*SOFL2; AT1G68870*)**,** (D)

631 *CHAPERONIN 60 BETA* (*CPN60B*; *AT1G55490*), and (E) *CASEIN KINASE I-LIKE 8* (*CKL8*;
632 *AT5G43320*). (F) homeostatic reaction norms for transcripts significantly and negatively correlated
633 with rLA under both watering regimes. (G) to (J) Scatter plots illustrating negative and homeostatic
634 relationships (*P*-value < 0.05) between rLA under both well-watered (closed circles) and drought
635 conditions (open circles) (y-axis), and transcript abundance (FPKM; x-axis) of (G) AT5G60160, (H)
636 *AT4G15260***,** (I) *AT5G16800*, and (J) *RING-H2 GROUP F1A* (*RHF1A*; *AT4G14220*). For 3a and 3f,
637 Spearman's rank correlation coefficient ($r_{s;}$ y-axis) indicates the correlation between the rLA and the
638 natural variation in transcript abundance of each gene. In Figs B to E and G to J, data were fitted
639 using a linear regression model. Also, in panels b-e and g-j, filled circles depict the rLA of accessions
640 grown under well-watered conditions, while empty circles squares depict the rLA of accessions
641 grown under drought.
642

643 **Fig. 5.** Arabidopsis accessions that display leaf area homeostasis in response to drought, display
644 higher water use efficiency as defined by $\delta^{13}C$. **(A)** Scatter plot illustrating the positive relationship
645 (*P*-value < 0.05) between leaf area homeostasis in response to drought (leaf area plasticity index, y-
646 axis) and water use efficiency (x-axis) among Iberian Arabidopsis accessions used in this study. Data
647 were fitted to a linear regression model. Grey shadow represents the 95% CI of the fit regression line
648 (black). $\delta^{13}C$ data for the accessions were retrieved from Dittberner *et al.* (2018). Four different
649 quadrants are defined by two dashed lines: y = 0, which is the homeostatic point at which a change
650 in water availability does not affect relative leaf area (i.e., a plasticity index of 0), and the average
651 intrinsic water use efficiency (WUE_i, $\delta^{13}C$*;* x-axis). Data points depict individual accessions with
652 their respective labels. **(**B) The genetic basis of leaf area plasticity in response to drought and water
653 use efficiency. This plot depicts the respective relationship between the GWAS associations found
654 for the leaf area plasticity index in response to drought (y-axis) and those for WUE_i (Dittberner *et al.*,
655 2018) (x-axis). Data points represent individual SNPs. The y-axis and x-axis depict the extent of the
656 association with, respectively, leaf area plasticity, and WUE_i, as the negative logarithm of the p-value.
657 Dashed lines depict an arbitrary threshold for significance that is consistent across comparisons. (C)
658 Transcriptomic association with plastic leaf area responses to drought and WUE_i. Spearman's rank
659 correlation depicts the relationship between the association of the transcript abundance of each gene
660 in the Arabidopsis genome with leaf area plasticity in response to drought (r_s) on the y-axis and with
661 WUE_i on the x-axis. Dashed lines define an arbitrary threshold to consider transcripts correlated

662 positively ($r_s \geq 0.4$) or negatively ($r_s \leq -0.4$) associated with leaf area plasticity (y-axis) or WUE_i (x-
663 axis). *CBF5* and *CNGC16* exemplify transcripts with opposing relationships to leaf area plasticity
664 and water use efficiency as shown in 4C, D and E. Scatter plots depicting the relationship (P-value <
665 0.05) between leaf area plasticity index in response to drought (4D), or water use efficiency (4E) on
666 the y-axis, and transcript abundance (FPKM) of *CBF5* on the x-axis. F and G. Scatter plots depicting
667 the relationship (*P*-value < 0.05) between (4F) leaf area plasticity index in response to drought or
668 (4G) water use efficiency (Dittberner *et al.*, 2018) on the y-axis, and transcript abundance (FPKM)
669 of *CYCLIC NUCLEOTIDE-GATED CHANNEL 16* (*CNGC16*) on the x-axis. In all panels, data were
670 fitted using a linear regression model. Grey shadow represents the 95% CI of the fit regression line.

671

672 **Fig. 6.** Photosynthesis-related transcript variants regulate water use efficiency in Iberian Arabidopsis
673 accessions**. (**A) Manhattan plot representing the genome-wide strength of association between genetic
674 variation and variation in $\delta^{13}C$ present within 95 Iberian accessions with $\delta^{13}C$ values available from
675 Dittberner *et al*. (2018). The score (y-axis) consists of the negative logarithm of the *P*-value and
676 provides association strength. Inset: Violin plots representing the probability densities of WUE_i for
677 the major and minor allele haplotypes in *ClpX* for the accessions included in Fig. 6A. (B) T-
678 Manhattan plot representing transcriptome-wide strength of association between variation in
679 transcript abundance (Kawakatsu *et al.*, 2016) and natural variation in $\delta^{13}C$. This analysis was
680 performed on all Iberian accessions with both transcript abundance data (Kawakatsu *et al.*, 2016) and
681 $\delta^{13}C$ information (Dittberner *et al.*, 2018) (n = 88 accessions). The relationship is defined by the
682 Spearman's rank correlation coefficient (r_s). Dashed lines define an arbitrary threshold for positive
683 ($r_s \geq 0.4$) or negative ($r_s \leq -0.4$) correlation with water-use efficiency (y-axis). Blue labels highlight
684 the transcripts positively associated with higher WUE_i, while red labels highlight those negatively
685 associated with higher WUE_i. (C) Hierarchical clustering tree summarizing the correlation among
686 significant GO Biological Process categories resulting from analysis of the positively correlated
687 candidates resulting from TWA analysis of water use efficiency determined from $\delta^{13}C$ values in 88
688 Iberian Arabidopsis accessions. Ratios provide the number of genes positively correlated with WUE_i
689 within each GO category relative to the total number of genes within that category. The size of the
690 blue dots increases proportionally with P-value significance. (D) Scatter plot depicting the positive
691 relationship (*P*-value < 0.05) between WUE_i (y-axis) and *RuBisCO SMALL SUBUNIT 2B*
692 (*AT5G38420*; *RBCS2B*) transcript abundance (x-axis) for the Iberian accessions included in Fig. 6B.

693 **(**E**)** Scatter plot depicting the positive relationship (*P*-value < 0.05) between intrinsic water-use
694 efficiency (WUE_i; y-axis) and *SMALL AUXIN UP RNA 26* (*SAUR26,* AT3G03850) transcript
695 abundance (x-axis) for the Iberian accessions included in 6b. Inset: Scatter plot depicting the positive
696 relationship (*P*-value < 0.05) between intrinsic water-use efficiency (WUE_i; y-axis) and *SMALL*
697 *AUXIN UP RNA 26* (*SAUR26,* AT3G03850) transcript abundance (x-axis) for the 43 accessions
698 included in our study. For 5D, and 5E, gray shadow represents the 95% CI of the fit regression line
699 (black).

700 # Tables

701 **Table 1.** List of 31 genes corresponding to the top 50 candidate SNPs with the strongest association
702 with the leaf area plasticity index. Genes encoding proteins with auxin-related functions from GO
703 analysis are bolded; additional genes related to auxin based on literature analysis are underlined.

Chr	Position	MAF (%)	Gene ID	Gene description	Label
5	**4892996**	**38.24**	***AT5G15100***	***Auxin efflux carrier family protein***	***PIN8***
3	1787622	26.47	*AT3G05970*	*long-chain acyl-CoA synthetase 6*	*LACS6*
4	**14703801**	**26.47**	***AT4G30080***	***auxin response factor 16***	***ARF16***
4	**14705049**	**26.47**	***AT4G30080***	***auxin response factor 16***	***ARF16***
5	5238732	23.53	*AT5G16030*	*mental retardation GTPase activating protein*	*AT5G16030*
3	975320	32.35	*AT3G03810*	*O-fucosyltransferase family protein*	*EDA30*
3	970856	20.59	*AT3G03800*	*syntaxin of plants 131*	*SYP131*
5	15293597	26.47	*AT5G38280*	*PR5-like receptor kinase*	*PR5K*
5	15293610	26.47	*AT5G38280*	*PR5-like receptor kinase*	*PR5K*
5	15293481	41.18	*AT5G38280*	*PR5-like receptor kinase*	*PR5K*
4	14691629	35.29	*AT4G30060*	*Core-2/I-branching beta-1,6-N-acetylglucosaminyltransferase family protein*	*AT4G30060*
5	4659907	35.29	*AT5G14450*	*GDSL-like Lipase/Acylhydrolase superfamily protein*	*AT5G14450*
5	18974632	20.59	*AT5G46760*	*Basic helix-loop-helix (bHLH) DNA-binding family protein*	*MYC3*
5	18974915	20.59	*AT5G46760*	*Basic helix-loop-helix (bHLH) DNA-binding family protein*	*MYC3*
5	18975625	20.59	*AT5G46760*	*Basic helix-loop-helix (bHLH) DNA-binding family protein*	*MYC3*
5	18975826	20.59	*AT5G46760*	*Basic helix-loop-helix (bHLH) DNA-binding family protein*	*MYC3*
3	**983189**	**38.24**	***AT3G03850***	***SAUR-like auxin-responsive protein family***	***SAUR26***
3	**983517**	**38.24**	***AT3G03850***	***SAUR-like auxin-responsive protein family***	***SAUR26***
3	1798927	29.41	*AT3G05990*	*Leucine-rich repeat (LRR) family protein*	*AT3G05990*
5	4433730	29.41	*AT5G13740*	*zinc induced facilitator 1*	*ZIF1*
5	4433740	29.41	*AT5G13740*	*zinc induced facilitator 1*	*ZIF1*
5	4436472	29.41	*AT5G13740*	*zinc induced facilitator 1*	*ZIF1*
5	4436745	29.41	*AT5G13740*	*zinc induced facilitator 1*	*ZIF1*
5	4442005	29.41	*AT5G13760*	*Plasma-membrane choline transporter family protein*	*AT5G13760*
5	**4450177**	**29.41**	***AT5G13790***	***AGAMOUS-like 15***	***AGL15***
5	**4450180**	**29.41**	***AT5G13790***	***AGAMOUS-like 15***	***AGL15***
2	13323264	23.53	*AT2G31260*	*autophagy 9*	*APG9*
2	13330862	23.53	*AT2G31270*	*CDT1-like protein A*	*CDT1A*
2	13341047	23.53	*AT2G31280*	*transcription factor bHLH155-like protein*	*LL2*
2	13341186	23.53	*AT2G31280*	*transcription factor bHLH155-like protein*	*LL2*
2	13342866	23.53	*AT2G31280*	*transcription factor bHLH155-like protein*	*LL2*
2	13343940	23.53	*AT2G31290*	*Ubiquitin carboxyl-terminal hydrolase family protein*	*AT2G31290*
2	13345229	23.53	*AT2G31290*	*Ubiquitin carboxyl-terminal hydrolase family protein*	*AT2G31290*
2	13345701	23.53	*AT2G31290*	*Ubiquitin carboxyl-terminal hydrolase family protein*	*AT2G31290*
2	13346191	23.53	*AT2G31300*	*actin-related protein C1B*	*ARPC1B*
2	13358923	23.53	*AT2G31320*	*poly(ADP-ribose) polymerase 2*	*PARP1*

3	22329843	23.53	*AT3G60400*	*Mitochondrial transcription termination factor family protein*	*SHOT1*
4	14775183	32.35	*AT4G30190*	*H[+]-ATPase 2*	*AHA2*
4	6154596	32.35	*AT4G09770*	*TRAF-like family protein*	*AT4G09770*
1	29310771	20.59	*AT1G77960*	*repressor ROX1-like protein*	*AT1G77960*
5	18596240	20.59	*AT5G45840*	*Leucine-rich repeat protein kinase family protein*	*AT5G45840*
5	18604234	20.59	*AT5G45860*	*PYR1-like 11*	*PYL11*
5	18606400	20.59	*AT5G45870*	*PYR1-like 12*	*PYL12*
5	18606524	20.59	*AT5G45870*	*PYR1-like 12*	*PYL12*
5	18606721	20.59	*AT5G45870*	*PYR1-like 12*	*PYL12*
5	18606940	20.59	*AT5G45870*	*PYR1-like 12*	*PYL12*
5	18606953	20.59	*AT5G45870*	*PYR1-like 12*	*PYL12*
5	**18613579**	**20.59**	***AT5G45890***	***senescence-associated gene 12***	***SAG12***
5	3708088	20.59	*AT5G11550*	*ARM repeat superfamily protein*	*AT5G11550*
5	4655788	20.59	*AT5G14430*	*S-adenosyl-L-methionine-dependent methyltransferases superfamily protein*	*AT5G14430*

Supporting information

The following supplemental materials are available:

Fig. S1. Rosette leaf area observations at the time of flowering (Table P1).

Fig. S2. Quantile-quantile (QQ) plots for GWAS analysis using the Linear Model.

Fig. S3. Quantile-quantile (QQ) plots for GWAS analysis using the Accelerated Mixed Model.

Fig. S4. Quantile-quantile (QQ) plots for GWAS analysis using GWAS-Flow.

Fig. S5. Histograms of the distribution of r_s and scores obtained from GWA and TWA analyses of the traits discussed in this study illustrate the stringent significance thresholds imposed in this study (vertical dashed lines).

Fig. S6. The plasticity index that we calculated is predictive of the percentage change in leaf area under drought relative to well-watered conditions.

Fig. S7. The identification of our candidate genes upon application of several different GWAS methods improves confidence in candidates for leaf area plasticity and intrinsic water use efficiency (WUE_i).

Fig. S8. Genotypic and transcriptomic reaction norms based on the strength of association of individual SNPs and transcripts highlight the variation in the strength of these associations depending on water availability.

Fig. S9. The genetic and transcriptomic basis of the relationship between leaf area plasticity potential in response to drought with (Figs S9A, B) leaf area potential and (Figs S9C, D) intrinsic water use efficiency (WUE_i).

727 **Fig. S10.** Illustration of candidate transcript variants that regulate intrinsic water use efficiency in
728 Iberian Arabidopsis accessions.
729 **Table P1.** Leaf area measurements recorded in this experiment (well-watered and drought).
730 Calculated relative leaf area (rLA) and plasticity, water use efficiency (WUE_i, $\delta^{13}C$) values recorded
731 by Dittberner *et al.* (2018) and MOD17A2 (net primary productivity) information obtained from
732 AraCLIM (Ferrero-Serrano & Assmann, 2019) for the accessions included in our study.
733 **Table P2.** Water use efficiency (WUE_i, $\delta^{13}C$) values recorded by Dittberner *et al.* (2018) for 95
734 Iberian Arabidopsis accessions.
735 **Table G1.** Candidates obtained from GWAS on relative leaf area (rLA) under well-watered
736 conditions. Only associations with a score ≥ 4 are included here. For a raw, unfiltered, as well as for
737 a fully filtered and annotated (see Materials & Methods) version of this GWAS output, please visit
738 the data repository.
739 **Table G2.** Candidates obtained from GWAS on relative leaf area (rLA) under drought. Only
740 associations with a score ≥ 4 are included here. For a raw, unfiltered, as well as for a fully filtered
741 and annotated (see Materials & Methods) version of this GWAS output, please visit the data
742 repository.
743 **Table G3.** Candidates obtained from GWAS on leaf area plasticity. Only associations with a score ≥
744 4 are included here. For a raw, unfiltered, as well as for a fully filtered and annotated (see Materials
745 & Methods) version of this GWAS output, please visit the data repository.
746 **Table G4.** Candidates obtained from GWAS on water use efficiency (WUE_i, δ13C) values recorded
747 by Dittberner *et al.* (2018) for the accessions included in our study. Only associations with a score ≥
748 4 are included here. For a raw, unfiltered, as well as for a fully filtered and annotated (see Materials
749 & Methods) version of this GWAS output, please visit the data repository.
750 **Table G5**. Candidates obtained from GWAS on water use efficiency (WUE_i, δ13C) values recorded
751 by Dittberner *et al.* (2018) for 95 Iberian Arabidopsis accessions. Only associations with a score ≥ 4
752 are included here. For a raw, unfiltered, as well as for a fully filtered and annotated (see Materials &
753 Methods) version of this GWAS output, please visit the data repository.
754 **Table G6.** Candidates obtained from eGWAS on the natural variation in transcript abundance of
755 *SAUR26* extracted from Kawakatsu *et al.* (2016). For a raw, unfiltered, as well as for a fully filtered
756 and annotated (see Materials & Methods) version of this GWAS output, please visit the data
757 repository.

758 **Table T1**. Results from TWAS (r_s).

759 **Table T2.** Results from TWAS (*P*-value).

760 **Table GO1.** GO analysis on the 31 genes corresponding to the top 50 candidate SNPs resulting from
761 GWAS analysis on leaf area plasticity index for drought.

762 **Table GO2.** GO analysis on the 58 genes identified from TWAS to exhibit transcript abundances
763 that are negatively correlated with leaf area plasticity index for drought, and negatively correlated
764 with water use efficiency determined from ($\delta^{13}C$) values from accessions overlapping with our sample
765 (red datapoints in Fig. 5C).

766 **Table GO3.** GO analysis on the 45 genes identified from TWAS to exhibit transcript abundances
767 that are positively correlated with water use efficiency determined from ($\delta^{13}C$) values in 88 Iberian
768 Arabidopsis accessions (datapoints with $r_s \geq 0.4$ in Fig. 6B).

769 **Table GO4.** GO analysis on the 494 genes identified from TWAS to exhibit transcript abundances
770 that are positively correlated with leaf area plasticity index for drought (green and grey datapoints
771 with $r_s \geq 0.4$ in the y-axis representing leaf area plasticity index in Fig. 5C).

772 **Table GO5.** GO analysis on the 28 genes identified from TWAS to exhibit transcript abundances
773 that are negatively correlated with relative leaf area (rLA) under well-watered conditions, and
774 positively correlated with leaf area plasticity index for drought (blue datapoints in S9B).

775 **Table GO6.** GO analysis on the 11 genes identified from TWAS to exhibit transcript abundances
776 that are negatively correlated with water use efficiency determined from ($\delta^{13}C$) values in 88 Iberian
777 Arabidopsis accessions (datapoints with $r_s \leq -0.4$ in Figure 6B).

778 **Table GO7.** GO analysis on the 302 genes identified from TWAS to exhibit transcript abundances
779 that are positively correlated with relative leaf area (rLA) under drought.

780 **Table GO8.** GO analysis on the 134 genes identified from TWAS to exhibit transcript abundances
781 that are negatively correlated with relative leaf area (rLA) under well-watered conditions (blue and
782 grey datapoints with $r_s \leq 0.4$ in the x-axis of Figure S9B).

783 **Table GO9**. GO analysis on the 177 genes identified from TWAS to exhibit transcript abundances
784 that are positively correlated with relative leaf area (rLA) under well-watered conditions (yellow and
785 grey datapoints with $r_s \geq 0.4$ in the x-axis of Figures S9B).

786 **Table GO10.** GO analysis on the 233 genes identified from TWAS that exhibit transcript abundances
787 which are negatively correlated with relative leaf area (rLA) under drought.

788

Acknowledgements

This research was supported by funding from The Pennsylvania State University to S.M.A. We thank Mr. Leland Burghard, Ms. Sarah Cronk, and Dr. Yotam Zait for greenhouse assistance. We thank Drs. David Chakravorty and Yotam Zait for helpful comments on the manuscript.

Author contributions

S.M.A & A.F-S. conceived the project, research plans, and experimental design. A.F-S. performed the experiments while S.M.A provided guidance throughout the experimental work. A.F-S. analyzed the data and prepared the figures; S.M.A supervised data analysis and figure preparation. S.M.A & A.F-S wrote the manuscript. A.F-S agrees to serve as the author responsible for contact and ensuring communication and assistance with the reproducibility of the results of this study.

Data Availability

The data supporting the results are available as Supporting Information files. The code and data to easily reproduce the analysis, figures, and tables in this manuscript are available at https://github.com/AssmannLab and will be uploaded to Zenodo upon acceptance.

References

Abudayyeh OO, Gootenberg JS, Essletzbichler P, Han S, Joung J, Belanto JJ, Verdine V, Cox DBT, Kellner MJ, Regev A, *et al.* 2017. RNA targeting with CRISPR-Cas13. Nature **550**, 280–284.

Angert AL, Huxman TE, Chesson P, Venable DL. 2009. Functional tradeoffs determine species coexistence via the storage effect. Proceedings of the National Academy of Sciences, U.S.A. **106**, 11641–11645.

Billings WD, Mooney HA. 1968. The ecology of arctic and alpine plants. Biological Reviews **43**, 481–529

Bradshaw AD. 1965. Evolutionary significance of phenotypic plasticity in plants. Elsevier, pp 115–155.

Castilla AR, Méndez-Vigo B, Marcer A, Martínez-Minaya J, Conesa D, Picó FX, Alonso-Blanco

817 **C.** 2020. Ecological, genetic and evolutionary drivers of regional genetic differentiation in
818 *Arabidopsis thaliana*. BMC Evolutionary Biology **20**, 1-13.
819 **Chapin, FS.** 1991. Integrated responses of plants to stress. Bioscience **41**, 29–36.
820 **Cheng, CY, Krishnakumar, V, Chan, AP, Thibaud-Nissen, F, Schobel, S, & Town, CD.** 2017.
821 Araport11: a complete reannotation of the *Arabidopsis thaliana* reference genome. The Plant
822 Journal **89**, 789-804.
823 **Cheng X, Fang T, Zhao E, Zheng B, Huang B, An Y, Zhou P.** 2020. Protective roles of salicylic
824 acid in maintaining integrity and functions of photosynthetic photosystems for alfalfa
825 (*Medicago sativa L.*) tolerance to aluminum toxicity. Plant Physiology and Biochemistry **155**
826 570-578.
827 **Cingolani P, Platts A, Wang LL, Coon M, Nguyen T, Wang L, Land SJ, Lu X, Ruden DM.**
828 2012. A program for annotating and predicting the effects of single nucleotide
829 polymorphisms, SnpEff: SNPs in the genome of *Drosophila melanogaster* strain w1118; iso-
830 2; iso-3. Fly (Austin) **6**, 80–92.
831 **Coll JR, Aguilar E, Ashcroft L.** 2016. Drought variability and change across the Iberian Peninsula.
832 Theoretical and Applied Climatology **130**, 901-916.
833 **Condon AG, Richards RA, Rebetzke GJ, Farquhar GD.** 2002. Improving intrinsic water-use
834 efficiency and crop yield. Crop Science **42**, 122–131.
835 **DeFalco TA, Moeder W, Yoshioka K.** 2016. Opening the gates: insights into cyclic nucleotide-
836 gated channel-mediated signaling. Trends in Plant Science **21**, 903–906.
837 **Des Marais DL, McKay JK, Richards JH, Sen S, Wayne T, Juenger TE.** 2012. Physiological
838 genomics of response to soil drying in diverse Arabidopsis accessions. Plant Cell **24**, 893–
839 914.
840 **Dhingra Y, Lahiri M, Bhandari N, Kaur I, Gupta S, Agarwal M, Katiyar-Agarwal S.** 2023.
841 Genome-wide identification, characterization, and expression analysis unveil the roles of
842 pseudouridine synthase (PUS) family proteins in rice development and stress
843 response. Physiology and Molecular Biology of Plants **29**, 1981-2004.
844 **Dittberner H, Korte A, Mettler-Altmann T, Weber APM, Monroe G, de Meaux J.** 2018. Natural
845 variation in stomata size contributes to the local adaptation of water-use efficiency in
846 *Arabidopsis thaliana*. Molecular Ecology **27**, 4052–4065.
847 **Donat MG, Lowry AL, Alexander LV, O'Gorman PA, Maher N.** 2016. More extreme

848 precipitation in the world's dry and wet regions. Nature Climate Change **6**, 508–513.
849 **Dorn LA, Pyle EH, Schmitt J.** 2000. Plasticity to light cues and resources in *Arabidopsis thaliana*:
850 testing for adaptive value and costs. Evolution **54**, 1982–1994.
851 **Easlon HM, Nemali KS, Richards JH, Hanson DT, Juenger TE, McKay JK.** 2014. The
852 physiological basis for genetic variation in water use efficiency and carbon isotope
853 composition in *Arabidopsis thaliana*. Photosynthesis Research **119**, 119–129.
854 **Emenecker, R. J., & Strader, L. C.** 2020. Auxin-abscisic acid interactions in plant growth and
855 development. Biomolecules **10**, 281.
856 **Exposito-Alonso M, 500 Genomes Field Experiment Team, Burbano HA, Bossdorf O, Nielsen**
857 **R, Weigel D.** 2019. Natural selection on the *Arabidopsis thaliana* genome in present and
858 future climates. *Nature* **573**, 126–129.
859 **Exposito-Alonso M, Brennan AC, Alonso-Blanco C, Picó FX.** 2018a. Spatio-temporal variation in
860 fitness responses to contrasting environments in *Arabidopsis thaliana*. Evolution **72**, 1570-
861 1586.
862 **Exposito-Alonso M, Vasseur F, Ding W, Wang G, Burbano HA, Weigel D.** 2018b. Genomic basis
863 and evolutionary potential for extreme drought adaptation in *Arabidopsis thaliana*. Nature
864 Ecology & Evolution **2**, 352–358.
865 **Ferguson JN, Fernandes SB, Monier B, Miller ND, Allan D, Dmitrieva A, Schmuker P, Lozano**
866 **R, Valluru R, Buckler ES, et al.** 2020. Machine learning enabled phenotyping for GWAS
867 and TWAS of WUE traits in 869 field-grown sorghum accessions. Plant Physiology
868 10.1093/plphys/kiab346.
869 **Ferrero-Serrano Á, Assmann SM.** 2019. Phenotypic and genome-wide association with the local
870 environment of Arabidopsis. Nature Ecology & Evolution **3**, 274–285.
871 **Ferrero-Serrano Á, Assmann SM.** 2016. The α-subunit of the rice heterotrimeric G protein, RGA1,
872 regulates drought tolerance during the vegetative phase in the dwarf rice mutant *d1*. Journal
873 of Experimental Botany **67**, 3433–3443.
874 **Ferrero-Serrano Á, Cantos C, Assmann SM.** 2019. The role of dwarfing traits in historical and
875 modern agriculture with a focus on rice. Cold Spring Harbor Perspectives in Biology, **11**,
876 p.a034645.
877 **Ferrero-Serrano Á, Chakravorty D, Kirven KJ, Assmann SM.** 2024. Oryza CLIMtools: A
878 genome–environment association resource reveals adaptive roles for heterotrimeric G

879 proteins in the regulation of rice agronomic traits. Plant Communications. 100813.
880 **Ferrero-Serrano, Á, Chakravorty D.** 2023. Plants and heterotrimeric G proteins: Expect the
881 unexpected. Molecular plant, ***16*****,** 506-508.
882 **Ferrero-Serrano Á, Sylvia MM, Forstmeier, PC, Olson, AJ, Ware, D, Bevilacqua, PC,**
883 **Assmann, SM.** 2022. Experimental demonstration and pan-structurome prediction of
884 climate-associated riboSNitches in Arabidopsis. Genome biology, **23**, 101.
885 **Ferrero-Serrano Á, Su Z, Assmann SM.** 2018. Illuminating the role of the Gα heterotrimeric G
886 protein subunit, *RGA1*, in regulating photoprotection and photoavoidance in rice. Plant, Cell
887 & Environment **41**, 451–468.
888 **Forsman A.** 2015. Rethinking phenotypic plasticity and its consequences for individuals, populations
889 and species. Heredity **115**, 276–284.
890 **Frachon L, Bartoli C, Carrère S, Bouchez O, Chaubet A, Gautier M, Roby D, Roux F.** 2018. A
891 genomic map of climate adaptation in *Arabidopsis thaliana* at a micro-geographic scale.
892 Frontiers in Plant Sciences **9**, 967.
893 **Frachon L, Mayjonade B, Bartoli C, Hautekèete N-C, Roux F.** 2019. Adaptation to plant
894 communities across the genome of *Arabidopsis thaliana*. Molecular Biology & Evolution **36**,
895 1442–1456.
896 **Freudenthal, JA, Ankenbrand, MJ, Grimm, DG, & Korte, A.** 2019. GWAS-Flow: A GPU
897 accelerated framework for efficient permutation based genome-wide association studies.
898 *BioRxiv.* doi: 10.1101/783100.
899 **Ge SX, Jung D, Yao R.** 2020. ShinyGO: a graphical gene-set enrichment tool for animals and plants.
900 Bioinformatics **36**, 2628–2629.
901 **Gomaa NH, Montesinos-Navarro A, Alonso-Blanco C, Picó FX.** 2011. Temporal variation in
902 genetic diversity and effective population size of Mediterranean and subalpine *Arabidopsis*
903 *thaliana* populations. Molecular Ecology **20**, 3540–3554.
904 **Grime, JP.** 1974. Vegetation classification by reference to strategies. Nature **250**, 26–31.
905
906 **Grime JP.** 1977. Evidence for the existence of three primary strategies in plants and its relevance to
907 ecological and evolutionary theory. The American Naturalist **111**, 1169–1194.
908 **Groszmann M, Osborn HL, Evans JR.** 2017. Carbon dioxide and water transport through plant
909 aquaporins. Plant, Cell & Environment **40**, 938–961.
910 **Gusev A, Ko A, Shi H, Bhatia G, Chung W, Penninx BWJH, Jansen R, de Geus EJC, Boomsma**

DI, Wright FA, *et al.* 2016. Integrative approaches for large-scale transcriptome-wide association studies. Nature Genetics **48**, 245–252.

Haldrup A, Naver H, Scheller HV. 1999. The interaction between plastocyanin and photosystem I is inefficient in transgenic Arabidopsis plants lacking the *PSI-N* subunit of photosystem I. The Plant Journal **17**, 689–698.

Harrell Jr F, Dupont C. 2019. Package 'Hmisc'. CRAN2018 2019: 235–6.

Heinsch FA, Reeves M, Votava P, Kang S, Milesi C, Zhao M, Glassy J, Jolly WM, Loehman R, Bowker CF, *et al.* 2003. Gpp and npp (mod17a2/a3) products nasa modis land algorithm. MOD17 User's Guide 1–57.

Hou, B, Lim, EK, Higgins, GS, Bowles, DJ. 2004. N-glucosylation of cytokinins by glycosyltransferases of Arabidopsis thaliana. *Journal of Biological Chemistry*, ***279***, 47822-47832.

Huang, L, He, B, Chen, A, Wang, H, Liu, J, Lű, A, & Chen, Z. 2016. Drought dominates the interannual variability in global terrestrial net primary production by controlling semi-arid ecosystems. Scientific reports ***6***, 1-7.

Ifuku K, Endo T, Shikanai T, Aro E-M. 2011. Structure of the chloroplast NADH dehydrogenase-like complex: nomenclature for nuclear-encoded subunits. Plant & Cell Physiology **52**, 1560–1568.

IRRI. 2021. Phenotyping protocols for abiotic stress tolerance in rice. International Rice Research Institute, Los Baños, Phillipines.

Juenger TE, McKay JK, Simms EI, Richards JH. 2005. Identification and characterization of QTL underlying whole-plant physiology in *Arabidopsis thaliana*: $\delta^{13}C$, stomatal conductance and transpiration efficiency. Plant, Cell & Environment **28**, 697–708.

Karijolich, J., Yi, C., & Yu, Y. T. 2015. Transcriptome-wide dynamics of RNA pseudouridylation. Nature reviews Molecular cell biology, **16**, 581-585.

Kasuga M, Liu Q, Miura S, Yamaguchi-Shinozaki K, Shinozaki K. 1999. Improving plant drought, salt, and freezing tolerance by gene transfer of a single stress-inducible transcription factor. Nature Biotechnology **17**, 287–291.

Kawakatsu T, Huang S-SC, Jupe F, Sasaki E, Schmitz RJ, Urich MA, Castanon R, Nery JR, Barragan C, He Y, *et al.* 2016. Epigenomic diversity in a global collection of *Arabidopsis thaliana* accessions. Cell **166**: 492–505.

942 **Kim J, Rudella A, Ramirez Rodriguez V, Zybailov B, Olinares PDB, van Wijk KJ.** 2009.
943 Subunits of the plastid ClpPR protease complex have differential contributions to
944 embryogenesis, plastid biogenesis, and plant development in Arabidopsis. The Plant Cell **21**,
945 1669–1692.
946 **Kimball S, Gremer JR, Angert AL, Huxman TE, Venable DL.** 2012. Fitness and physiology in a
947 variable environment. Oecologia ***169***, 319–329.
948 **Van Kleunen M, Fischer M.** 2005. Constraints on the evolution of adaptive phenotypic plasticity in
949 plants. New Phytologist **166**, 49–60.
950 **Köhler C, Merkle T, Neuhaus G.** 1999. Characterisation of a novel gene family of putative cyclic
951 nucleotide- and calmodulin-regulated ion channels in *Arabidopsis thaliana*. The Plant Journal
952 **18**, 97–104.
953 **Korte A, Farlow A.** 2013. The advantages and limitations of trait analysis with GWAS: a review.
954 Plant Methods **9**, 29.
955 **Kramer, MC, Janssen, KA, Palos, K, Nelson AD, Vandivier LE, Garcia BA, ..., Gregory BD.**
956 2020. N6-methyladenosine and RNA secondary structure affect transcript stability and
957 protein abundance during systemic salt stress in Arabidopsis. e00239
958 **Kremling KAG, Diepenbrock CH, Gore MA, Buckler ES, Bandillo NB.** 2019. Transcriptome-
959 wide association supplements genome-wide association in *Zea mays*. G3: Genes, Genomes,
960 Genetics **9**, 3023–3033.
961 **Lasky JR, Des Marais DL, Lowry DB, Povolotskaya I, McKay JK, Richards JH, Keitt TH,**
962 **Juenger TE.** 2014. Natural variation in abiotic stress responsive gene expression and local
963 adaptation to climate in *Arabidopsis thaliana*. Molecular Biology and Evolution **31**, 2283–
964 2296.
965 **Lermontova, I, Schubert, V, Börnke, F, Macas, J, & Schubert, I.** 2007. Arabidopsis CBF5
966 interacts with the H/ACA snoRNP assembly factor NAF1. Plant molecular biology ***65***, 615-
967 626.
968 **Leyser HM, Pickett FB, Dharmasiri S, Estelle M.** 1996. Mutations in the *AXR3* gene of
969 Arabidopsis result in altered auxin response including ectopic expression from the *SAUR-AC1*
970 promoter. The Plant Journal **10**, 403–413.
971 **Li Z-G, Chen H-W, Li Q-T, Tao J-J, Bian X-H, Ma B, Zhang W-K, Chen S-Y, Zhang J-S.** 2015.
972 Three SAUR proteins *SAUR76*, *SAUR77* and *SAUR78* promote plant growth in Arabidopsis.

973 Scientific Reports **5**, 12477.
974 **Li D, Liu Q, & Schnable, PS.** 2021. TWAS results are complementary to and less affected by
975 linkage disequilibrium than GWAS. Plant Physiology **186**, 1800-1811.
976 **Liu J, Zhang Y, Qin G, Tsuge T, Sakaguchi N, Luo G, Sun K, Shi D, Aki S, Zheng N, Aoyama**
977 **T.** 2008. Targeted degradation of the cyclin-dependent kinase inhibitor ICK4/KRP6 by
978 RING-type E3 ligases is essential for mitotic cell cycle progression during Arabidopsis
979 gametogenesis. *The Plant Cell*, ***20***,1538-1554.
980 **Livingston AK, Cruz JA, Kohzuma K, Dhingra A, Kramer DM.** 2010. An Arabidopsis mutant
981 with high cyclic electron flow around photosystem I (*hcef*) involving the NADPH
982 dehydrogenase complex. Plant Cell **22**, 221–233.
983 **Lobo JM, Castro I, Moreno JC.** 2001. Spatial and environmental determinants of vascular plant
984 species richness distribution in the Iberian Peninsula and Balearic Islands. Biological Journal
985 of the Linnean Society **73**, 233–253.
986 **Maiwald D, Dietzmann A, Jahns P, Pesaresi P, Joliot P, Joliot A, Levin JZ, Salamini F, Leister**
987 **D.** 2003. Knock-out of the genes coding for the Rieske protein and the ATP-synthase delta-
988 subunit of Arabidopsis. Effects on photosynthesis, thylakoid protein composition, and nuclear
989 chloroplast gene expression. Plant Physiology **133**, 191–202.
990 **Manzano-Piedras E, Marcer A, Alonso-Blanco C, Picó FX.** 2014. Deciphering the adjustment
991 between environment and life history in annuals: lessons from a geographically-explicit
992 approach in *Arabidopsis thaliana*. PLoS One 9, e87836.
993 **Marcer A, Vidigal DS, James PMA, Fortin MJ, Méndez-Vigo B, Hilhorst HWM, Bentsink L,**
994 **Alonso-Blanco C, Picó FX.** 2018. Temperature fine-tunes Mediterranean *Arabidopsis*
995 *thaliana* life-cycle phenology geographically. Plant Biology **20**, 148–156.
996 **Méndez-Vigo B, Picó FX, Ramiro M, Martínez-Zapater JM, Alonso-Blanco C.** 2011. Altitudinal
997 and climatic adaptation is mediated by flowering traits and FRI, FLC, and PHYC genes in
998 Arabidopsis. Plant Physiology **157**, 1942–1955.
999 **Montesinos A, Tonsor SJ, Alonso-Blanco C, Picó FX.** 2009. Demographic and genetic patterns of
1000 variation among populations of *Arabidopsis thaliana* from contrasting native environments.
1001 PLoS One 4, e7213.
1002 **Montesinos-Navarro A, Wig J, Pico FX, Tonsor SJ.** 2011. *Arabidopsis thaliana* populations show
1003 clinal variation in a climatic gradient associated with altitude. New Phytologist **189**, 282–294.

1004 **Murakami R, Ifuku K, Takabayashi A, Shikanai T, Endo T, Sato F.** 2005. Functional dissection
1005 of two Arabidopsis PsbO proteins: *PsbO1* and *PsbO2*. The FEBS Journal **272**, 2165–2175.
1006 **Nagatoshi Y, Ikeda M, Kishi H, Hiratsu K, Muraguchi A, Ohme-Takagi M.** 2016. Induction of
1007 a dwarf phenotype with IBH1 may enable increased production of plant-made
1008 pharmaceuticals in plant factory conditions. Plant Biotechnology Journal **14**, 887–894.
1009 **Nilson, S. E., & Assmann, S. M.** 2010. Heterotrimeric G proteins regulate reproductive trait
1010 plasticity in response to water availability. New Phytologist **185***,* 734-746.
1011 **Nishimura K, van Wijk KJ.** 2015. Organization, function and substrates of the essential Clp
1012 protease system in plastids. *Biochimica et Biophysica Acta* **1847**, 915–930.
1013 **Oh E, Zhu J-Y, Bai M-Y, Arenhart RA, Sun Y, Wang Z-Y.** 2014. Cell elongation is regulated
1014 through a central circuit of interacting transcription factors in the Arabidopsis hypocotyl.
1015 Elife. doi: 10.7554/eLife.03031.
1016 **Ohashi-Ito K, Matsukawa M, Fukuda H.** 2013. An atypical bHLH transcription factor regulates
1017 early xylem development downstream of auxin. Plant Cell Physiol **54**, 398–405.
1018 **Park SY, Scranton MA, Stajich JE, Yee A, Walling LL.** 2017. Chlorophyte aspartyl
1019 aminopeptidases: ancient origins, expanded families, new locations, and secondary
1020 functions. Plos one ***12***, p.e0185492.
1021 **Parsons RF.** 1968. The significance of growth-rate comparisons for plant ecology. The American
1022 Naturalist **102**, 595–597.
1023 **Páscoa P, Gouveia CM, Russo A, Trigo RM.** 2017. Drought Trends in the Iberian Peninsula over
1024 the Last 112 Years. Advances in Meteorology **2017**, 1–13.
1025 **Picó FX.** 2012. Demographic fate of *Arabidopsis thaliana* cohorts of autumn- and spring-germinated
1026 plants along an altitudinal gradient. Journal of Ecology **100**, 1009–1018.
1027 **Picó FX, Méndez-Vigo B, Martínez-Zapater JM, Alonso-Blanco C.** 2008. Natural genetic
1028 variation of *Arabidopsis thaliana* is geographically structured in the Iberian peninsula.
1029 Genetics **180**, 1009–1021.
1030 **Price AL, Zaitlen NA, Reich D, Patterson N.** 2010. New approaches to population stratification in
1031 genome-wide association studies. Nature Reviews Genetics **11**, 459–463.
1032 **Rey Benayas JM, Scheiner SM.** 2002. Plant diversity, biogeography and environment in Iberia:
1033 Patterns and possible causal factors. Journal of Vegetation Science **13**, 245.
1034 **Rivero RM, Kojima M, Gepstein A, Sakakibara H, Mittler R, Gepstein S, Blumwald E.** 2007.

1035 Delayed leaf senescence induces extreme drought tolerance in a flowering plant. Proceedings
1036 of the National Academy of Sciences **104**,19631-19636.
1037 **Running SW, Zhao M.** 2015. Daily GPP and annual NPP . MOD17A2/A3. products NASA Earth
1038 Observing System MODIS land algorithm. MOD17 User's Guide 2015, 1–28.
1039 **Salehin M, Li B, Tang M, Katz E, Song L, Ecker JR, Kliebenstein DJ, Estelle M.** 2019. Auxin-
1040 sensitive Aux/IAA proteins mediate drought tolerance in Arabidopsis by regulating
1041 glucosinolate levels. Nature Communications **10**, 4021.
1042 **Schindele A, Dorn A, Puchta H.** 2020. CRISPR/Cas brings plant biology and breeding into the fast
1043 lane. Current Opinion in Biotechnology **61**, 7–14.
1044 **Schweizer F, Fernández-Calvo P, Zander M, Diez-Diaz M, Fonseca S, Glauser G, Lewsey MG,**
1045 **Ecker JR, Solano R, Reymond P.** 2013. Arabidopsis basic helix-loop-helix transcription
1046 factors MYC2, MYC3, and MYC4 regulate glucosinolate biosynthesis, insect performance,
1047 and feeding behavior. Plant Cell **25**, 3117–3132.
1048 **Seren Ü, Vilhjálmsson BJ, Horton MW, Meng D, Forai P, Huang YS, Long Q, Segura V,**
1049 **Nordborg M.** 2012. GWAPP: a web application for genome-wide association mapping in
1050 Arabidopsis. Plant Cell **24**, 4793–4805.
1051 **Siepielski AM, Morrissey MB, Buoro M, Carlson SM, Caruso CM, Clegg SM, Coulson T,**
1052 **DiBattista J, Gotanda KM, Francis CD, *et al*.** 2017. Precipitation drives global variation in
1053 natural selection. Science **355**, 959–962.
1054 **Spartz AK, Ren H, Park MY, Grandt KN, Lee SH, Murphy AS, Sussman MR, Overvoorde PJ,**
1055 **Gray WM.** 2014. SAUR inhibition of PP2C-D Phosphatases activates plasma membrane H^+-
1056 ATPases to promote cell expansion in Arabidopsis. Plant Cell **26**, 2129–2142
1057 **Stortenbeker N, Bemer M. 2019.** The SAUR gene family: the plant's toolbox for adaptation of
1058 growth and development. Journal of Experimental Botany **70**, 17–27.
1059 **Tabas-Madrid D, Méndez-Vigo B, Arteaga N, Marcer A, Pascual-Montano A, Weigel D, Xavier**
1060 **Picó F, Alonso-Blanco C.** 2018. Genome-wide signatures of flowering adaptation to climate
1061 temperature: regional analyses in a highly diverse native range of *Arabidopsis thaliana*. Plant,
1062 Cell & Environment **41**, 1806–1820.
1063 **Tang, Y., Gao, C. C., Gao, Y., Yang, Y., Shi, B., Yu, J. L., ... & Chong, K.** 2020. OsNSUN2-
1064 mediated 5-methylcytosine mRNA modification enhances rice adaptation to high
1065 temperature. Developmental cell ***53***, 272-286.

Team RC. 2013. R: A language and environment for statistical computing.

The 1001 Genomes Consortium 2016. 1,135 Genomes reveal the global pattern of polymorphism in *Arabidopsis thaliana*. Cell **166**, 481–491.

Tilman D. 1988. Plant strategies and the dynamics and structure of plant communities. Princeton University Press.

Tunc-Ozdemir M, Tang C, Ishka MR, Brown E, Groves NR, Myers CT, Rato C, Poulsen LR, McDowell S, Miller G, *et al.* 2013. A cyclic nucleotide-gated channel (~~.~~CNGC16)~~.~~ in pollen is critical for stress tolerance in pollen reproductive development. Plant Physiology **161**, 1010–1020.

Via S, Gomulkiewicz R, De Jong G, Scheiner SM, Schlichting CD, Van Tienderen PH. 1995. Adaptive phenotypic plasticity: consensus and controversy. Trends in Ecology & Evolution. **10,** 212–217.

Vicente-Serrano SM. 2006a. Spatial and temporal analysis of droughts in the Iberian Peninsula. 1910–2000. Hydrological Sciences Journal **51**, 83–97

Vicente-Serrano SM. 2006b. Differences in spatial patterns of drought on different time scales: an analysis of the iberian peninsula. Water Resources Management **20**, 37–60.

Vidigal DS, Marques ACSS, Willems LAJ, Buijs G, Méndez-Vigo B, Hilhorst HWM, Bentsink L, Picó FX, Alonso-Blanco C. 2016. Altitudinal and climatic associations of seed dormancy and flowering traits evidence adaptation of annual life cycle timing in *Arabidopsis thaliana*. Plant, Cell & Environment **39**, 1737–1748.

Wang Y-F, Munemasa S, Nishimura N, Ren H-M, Robert N, Han M, Puzõrjova I, Kollist H, Lee S, Mori I, *et al.* 2013. Identification of cyclic GMP-activated nonselective Ca2+-permeable cation channels and associated *CNGC5* and *CNGC6* genes in Arabidopsis guard cells. Plant Physiology **163**, 578–590.

Wang Z, Yang L, Liu Z, Lu M, Wang M, Sun Q, Lan Y, Shi T, Wu D, Hua J. 2019. Natural variations of growth thermo-responsiveness determined by SAUR26/27/28 proteins in *Arabidopsis thaliana*. New Phytologist **224**, 291–305.

Wang Z, Yang L, Wu D, Zhang N, Hua J. 2021. Polymorphisms in cis-elements confer SAUR26 gene expression difference for thermo-response natural variation in Arabidopsis. New Phytologist **229**, 2751–2764.

1096 **Weijschedé, J, Martínková, J, De Kroon, H, & Huber, H.** 2006. Shade avoidance in *Trifolium*
1097 *repens*: costs and benefits of plasticity in petiole length and leaf size. New Phytologist ***172,***
1098 655-666.
1099 **West-Eberhard MJ.** 2003. Developmental plasticity and evolution. Oxford University Press
1100 **Wickham H, Francois R, Henry L, Müller K.** 2015. dplyr: A grammar of data manipulation. R
1101 package version 0.4 3.
1102 **Wickham H, Henry L.** 2018. tidyr: Easily Tidy Data with 'spread 'and 'gather'Functions. R package
1103 version 0.8 2.
1104 **Wolfe MD, Tonsor SJ.** 2014. Adaptation to spring heat and drought in northeastern Spanish
1105 *Arabidopsis thaliana*. New Phytologist **201**, 323–334.
1106 **Wong JH, Klejchová M, Snipes SA, Nagpal P, Bak G, Wang B, ..., Gray WM.** 2021. SAUR
1107 proteins and PP2C. D phosphatases regulate H^+-ATPases and K+ channels to control
1108 stomatal movements. Plant Physiology **185**, 256-273.
1109 **Yamori W, Sakata N, Suzuki Y, Shikanai T, Makino A.** 2011. Cyclic electron flow around
1110 photosystem I via chloroplast NAD. P.H dehydrogenase. NDH. complex performs a
1111 significant physiological role during photosynthesis and plant growth at low temperature in
1112 rice. Plant Journal **68**, 966–976.
1113 **Zait Y, Ferrero-Serrano Á & Assmann, SM.** 2021. The α subunit of the heterotrimeric G protein
1114 regulates mesophyll CO_2 conductance and drought tolerance in rice. New Phytologist, **232**,
1115 2324-2338.
1116 **Zhang, J, Vankova, R, Malbeck, J, Dobrev, PI, Xu, Y, Chong, K, Neff, MM.** 2009. *AtSOFL1* and
1117 *AtSOFL2* act redundantly as positive modulators of the endogenous content of specific
1118 cytokinins in Arabidopsis. *PLoS One*, ***4***, p.e8236.
1119 **Zhang H, Zhao Y, Zhu J-K.** 2020. Thriving under stress: how plants balance growth and the stress
1120 response. Developmental Cell **55**, 529–543.
1121 **Zhao Z, Zhang W, Stanley BA, Assmann SM.** 2008. Functional proteomics of *Arabidopsis thaliana*
1122 guard cells uncovers new stomatal signaling pathways. The Plant Cell, **20**, 3210-26.
1123 **Zheng Q, Zheng Y, Ji H, Burnie W, Perry SE.** 2016. Gene regulation by the *AGL15* transcription
1124 factor reveals hormone interactions in somatic embryogenesis. Plant Physiology **172**, 2374–
1125 2387.
1126

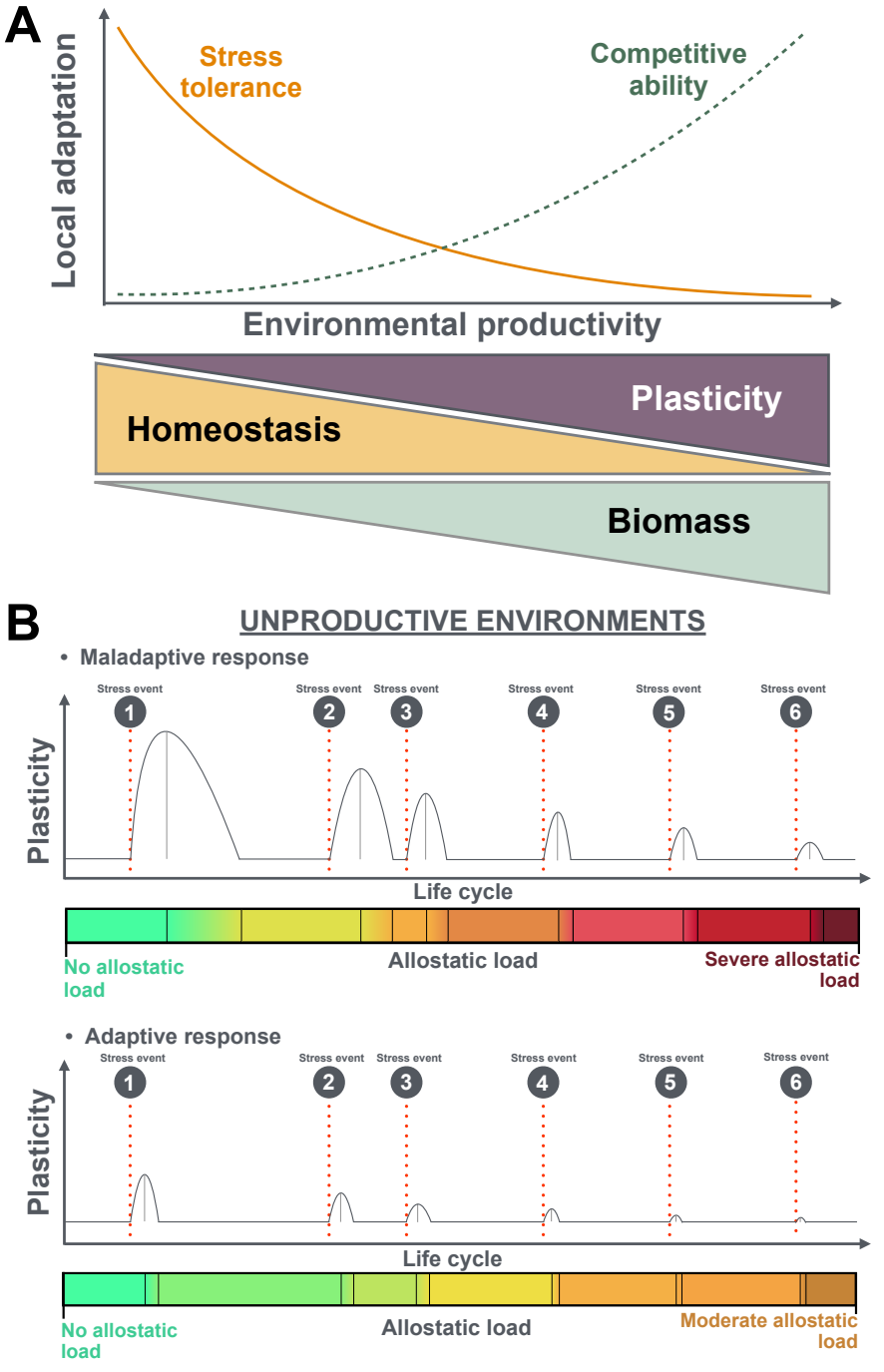

Fig 1. Conceptual framework for the adaptive role of plastic and homeostatic responses across productivity gradients in the local environment. (A) Schematic illustration representing the balance *sensu* Grime (1974, 1977), between stress tolerance in lower productivity, stress-prone environments, and competitive ability in and homeostasis in plants. In less productive environments, homeostatic responses to stress and lower relative growth rates result in lower biomass production, which is tuned in to the lower resources that are typically available in their environment and favors adaptation to those environments. In contrast, in productive environments, in which competition becomes more intense, plastic responses are favored from an adaptive standpoint. (B). In unproductive environments, frequent stress events can increase the allostatic load in individuals adapted to high-productivity environments where plastic responses are beneficial. During the lifetime of an individual, this results in a maladaptive response that increases allostatic load. In contrast, individuals adapted to unproductive environments exhibit less plastic (more homeostatic) responses to repeated stress that reduces their allostatic load over their lifetime.

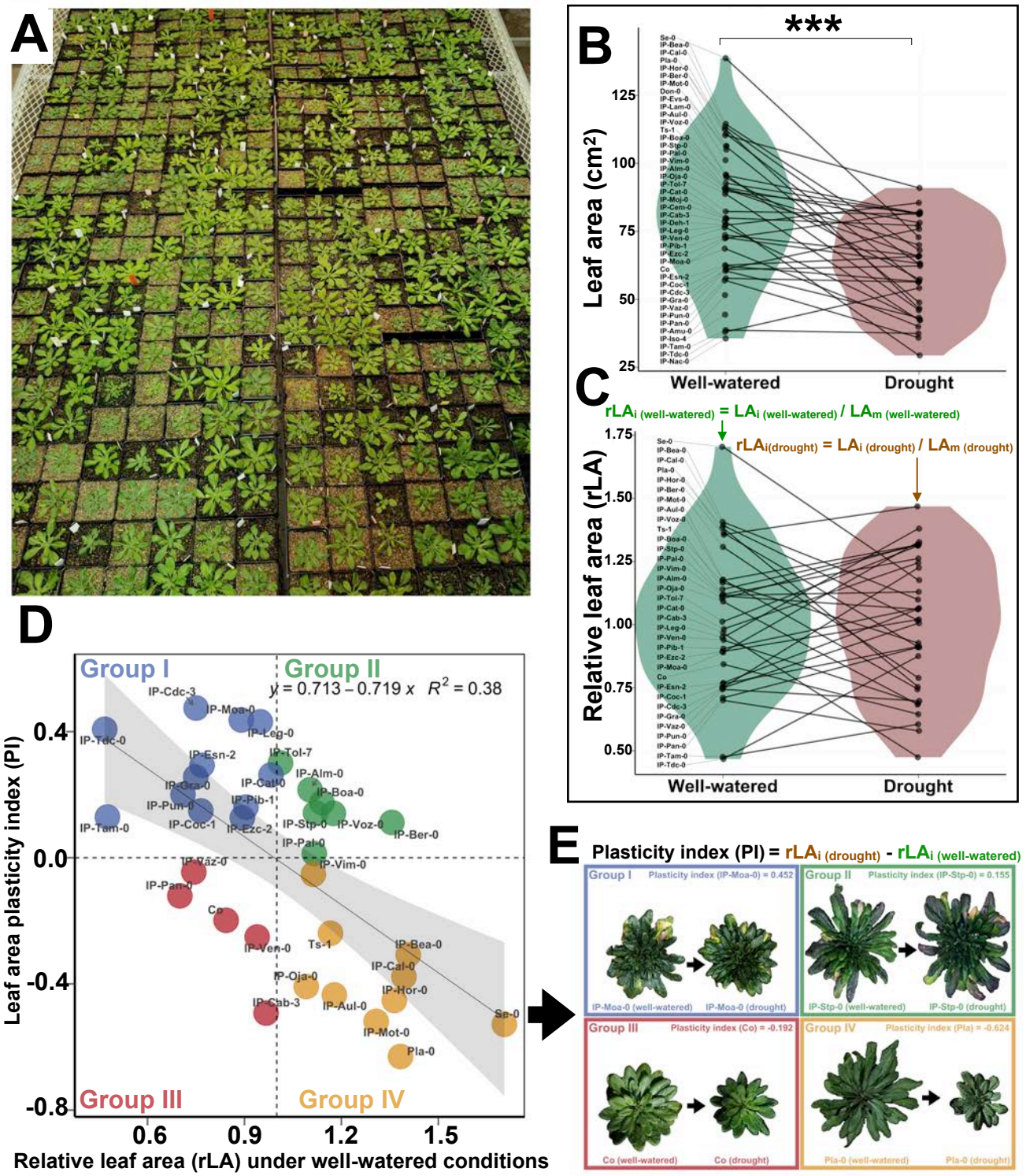

Fig. 2. Accession-specific rosette leaf area responses in Arabidopsis. (A) Detail of the common garden experiment, illustrating the randomization of well-watered and drought treatments, as reflected in soil coloration. (B) Phenotypic reaction norms illustrating a reduction of leaf area in response to drought in most but not all accessions. Violin distributions represent probability densities of leaf area (cm^2) among the accessions included in this study. Datapoints depict the mean phenotypic values of individual accessions, and the reaction norms represent the plastic response in the leaf area of each accession in response to drought (t-test; P-value < 0.001). (C) Phenotypic reaction norms illustrating plastic and homeostatic responses in relative leaf area (rLA). Violin distributions represent probability densities of rLA among the accessions included in this study. Datapoints depict the rLA of individual accessions, and the reaction norms represent the plastic response in rLA of each accession in response to drought (t-test; P-value > 0.05). (D) Negative relationship (P-value < 0.05) between leaf area plasticity index (slope of the reaction norms in 2C) in response to drought (y-axis) and rLA under well-watered conditions (x-axis). Data were fitted using a linear regression model. Grey shadow represents the 95% CI of the fit regression line. Four different quadrants are defined by two dashed lines: the average rLA (x-axis), and y = 0, which is the homeostatic point at which a change in water availability does not affect rLA (i.e. a plasticity index of 0). Data points depict individual accessions with their respective label. Data points are colored based on in which quadrant they fall (see text). (E) Images illustrating the plastic and homeostatic responses to drought found among the accessions included in this study.

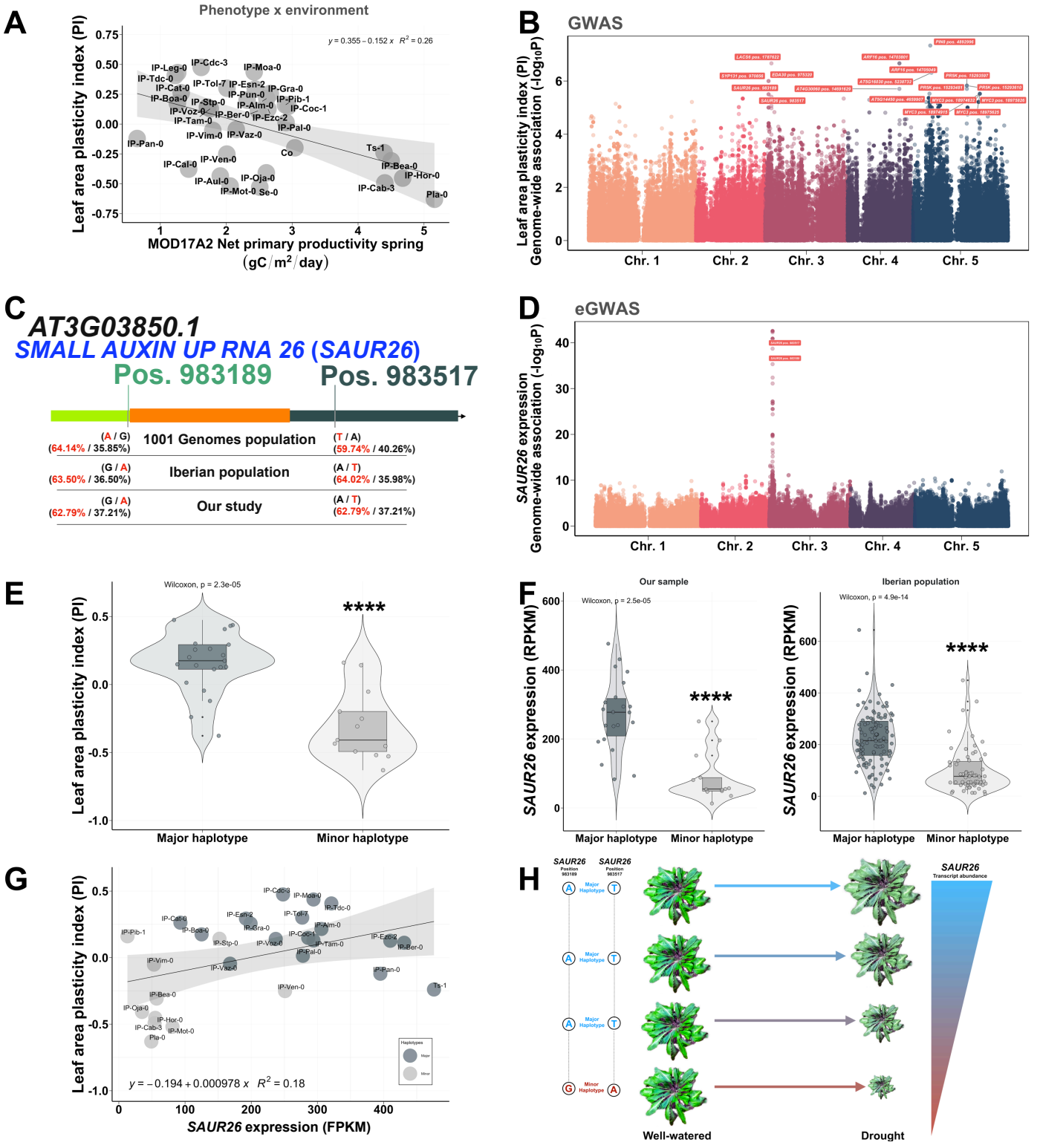

Fig. 3. *SMALL AUXIN UP RNA 26* (*SAUR26,* AT3G03850) is a candidate regulator of Arabidopsis leaf area plasticity in response to drought. (A) Accessions from more productive areas display stronger negative reductions in leaf area plasticity relative to accessions from less productive environments. Scatter plot depicting the negative relationship (P-value < 0.05) between leaf area plasticity index (y-axis) and Net Primary Productivity during the spring season (x-axis). (B) Manhattan plot representing the strength of association between genetic variants and leaf area plasticity in response to drought. (C) *SAUR26* gene model, including the two co-varying SNPs highlighted in 2B. Orange block depicts the sole exon, green block the 5' UTR, dark green block the 3' UTR. Labels above indicate the position of the two SNPs that co-vary, forming a haplotype in our sample. Major/minor allele frequency in our sample, in the 189 accessions from the Iberian Peninsula included in the 1001 Genome Project, and the whole 1001 Genomes Project sample dataset is provided. (D) Manhattan plot representing the genome-wide strength of association between the genetic variation present within the 665 accessions from the transcript abundance reference panel (Kawakatsu *et al.*, 2016) that overlap with the collection of accessions included in the 1001 Genomes Project, and the variation in the transcript abundance of *SAUR26* (Kawakatsu *et al.*, 2016). The peak in chromosome 3 represents the cis-genetic variants in *SAUR26* affecting its transcript abundance. For the Manhattan plots in 3B and D, the score (y-axis) consists of the negative logarithm of the P-value and provides association strength. Each data point represents a SNP with a color corresponding to the chromosome where the genetic variants are located. The x-axis and the different colors shown in the SNPs depicted in the Manhattan plots represent the different chromosomes. The higher the score, the lower the P-value, and the stronger the association between genetic variation and leaf area plasticity or *SAUR26* transcript abundance. (E) In the Iberian population, the major haplotype of *SAUR26* is associated with homeostatic or positive responses of relative leaf area (rLA) in response to drought. Conversely, the minor haplotype in the Iberian population is associated with plastic responses in rLA in response to drought. Violin plots show significantly different probability densities of leaf area plasticity in response to drought for the major and minor allele haplotypes in *SAUR26.* (F) The haplotypes in *SAUR26* associated with leaf area plasticity/homeostasis in response to drought are associated with differences in *SAUR26* gene expression. Violin plots show significantly different probability densities of *SAUR26* transcript abundance for the major and minor allele haplotypes in *SAUR26* for both our sample and the entire Iberian population. (G) Scatter plot illustrating the positive relationship between leaf area plasticity index (y-axis) and *SAUR26* transcript abundance (x-axis). For 2A and 2G, the grey shadow represents the 95% CI of the fit regression line (dark grey). (H) Cartoon illustrating the regulatory role of genetic and transcript variation in *SAUR26* and the response of leaf area to drought.

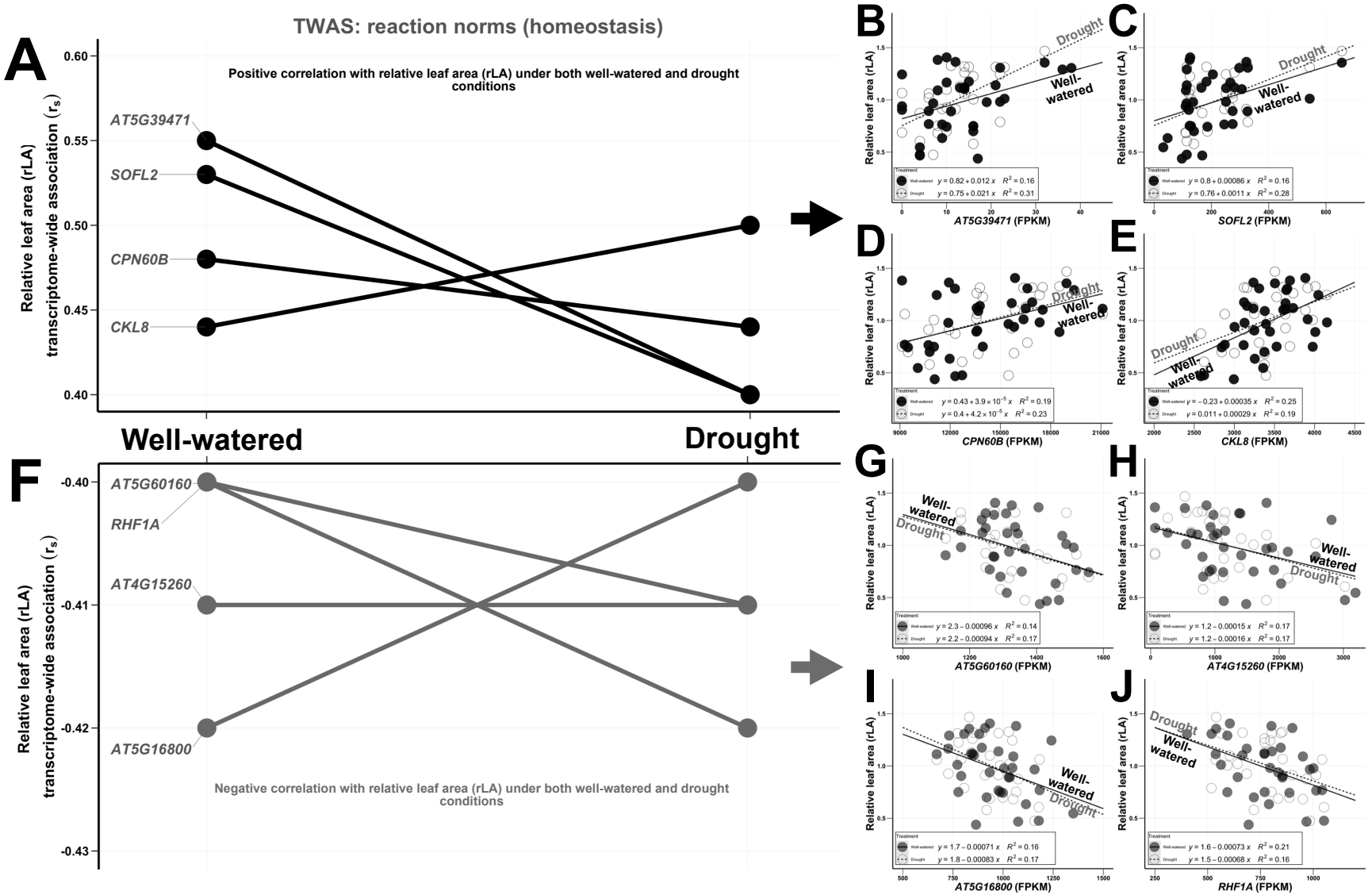

Fig. 4. Transcriptomic reaction norms uncover genetic correlates of Arabidopsis leaf area homeostasis in response to drought. (A) homeostatic reaction norms for transcripts significantly and positively correlated with relative leaf area (rLA) under both watering regimes. (B) to (E). Scatter plots illustrating positive and homeostatic relationships (P-value < 0.05) between rLA under both well-watered (closed circles) and drought conditions (open circles) conditions (y-axis), and transcript abundance (FPKM; x-axis) of (B) AT5G39471, (C) *SOB FIVE-LIKE 2* (*SOFL2; AT1G68870*)**,** (D) *CHAPERONIN 60 BETA* (*CPN60B*; *AT1G55490*), and (E) *CASEIN KINASE I-LIKE 8* (*CKL8*; *AT5G43320*). (F) homeostatic reaction norms for transcripts significantly and negatively correlated with rLA under both watering regimes. (G) to (J) Scatter plots illustrating negative and homeostatic relationships (P-value < 0.05) between rLA under both well-watered (closed circles) and drought conditions (open circles) (y-axis), and transcript abundance (FPKM; x-axis) of (G) AT5G60160, (H) *AT4G15260***,** (I) *AT5G16800*, and (J) *RING-H2 GROUP F1A* (*RHF1A*; *AT4G14220*). For 3a and 3f, Spearman's rank correlation coefficient ($r_{s;}$ y-axis) indicates the correlation between the rLA and the natural variation in transcript abundance of each gene. In Figs B to E and G to J, data were fitted using a linear regression model. Also, in panels b-e and g-j, filled circles depict the rLA of accessions grown under well-watered conditions, while empty circles squares depict the rLA of accessions grown under drought.

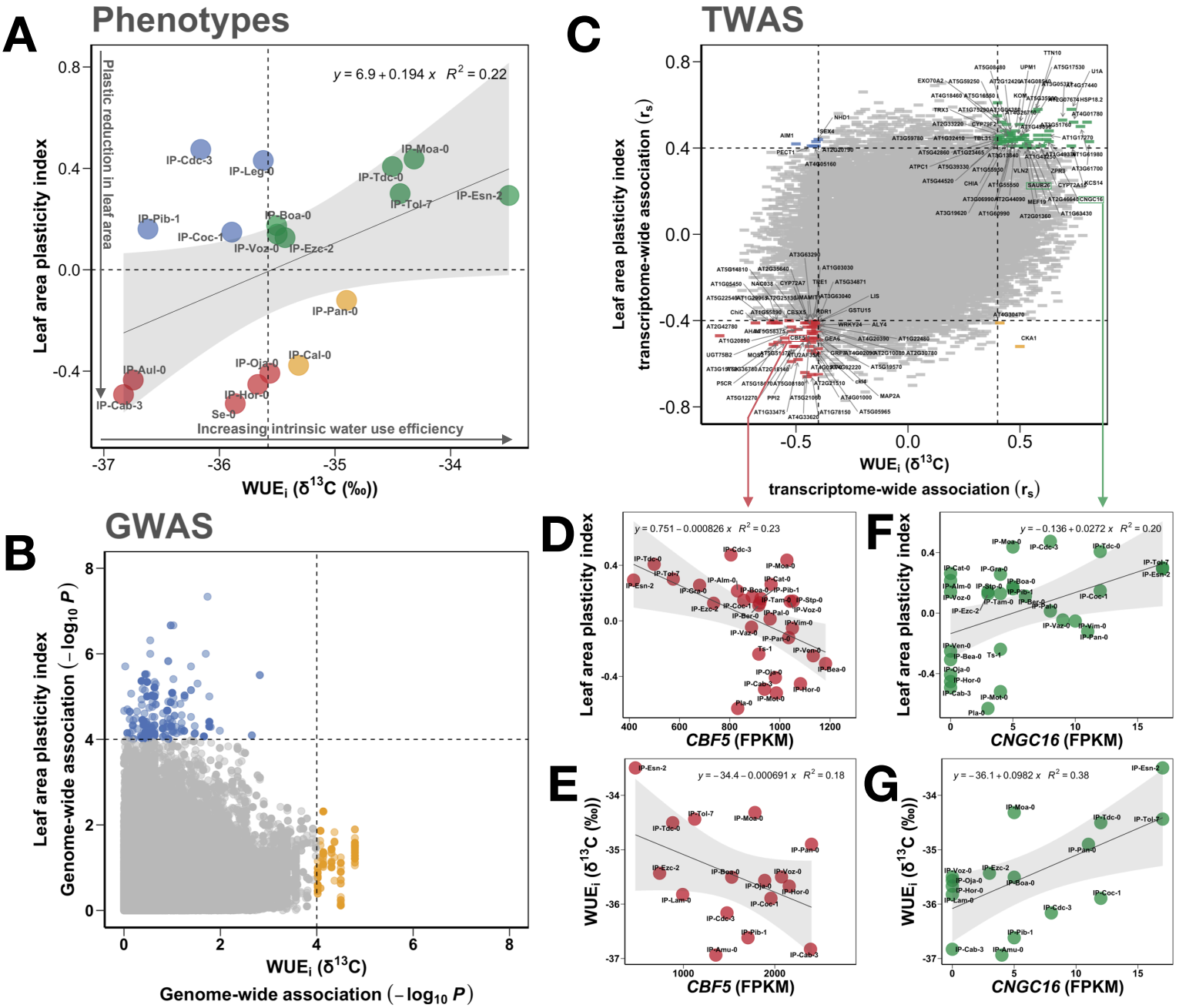

Fig. 5. Arabidopsis accessions that display leaf area homeostasis in response to drought, display higher water use efficiency as defined by $\delta^{13}C$. **(A)** Scatter plot illustrating the positive relationship (P-value < 0.05) between leaf area homeostasis in response to drought (leaf area plasticity index, y-axis) and water use efficiency (x-axis) among Iberian Arabidopsis accessions used in this study. Data were fitted to a linear regression model. Grey shadow represents the 95% CI of the fit regression line (black). $\delta^{13}C$ data for the accessions were retrieved from Dittberner *et al.* (2018). Four different quadrants are defined by two dashed lines: y = 0, which is the homeostatic point at which a change in water availability does not affect relative leaf area (i.e., a plasticity index of 0), and the average intrinsic water use efficiency (WUE_i, $\delta^{13}C$; x-axis). Data points depict individual accessions with their respective labels. **(B)** The genetic basis of leaf area plasticity in response to drought and water use efficiency. This plot depicts the respective relationship between the GWAS associations found for the leaf area plasticity index in response to drought (y-axis) and those for WUE_i (Dittberner *et al.*, 2018) (x-axis). Data points represent individual SNPs. The y-axis and x-axis depict the extent of the association with, respectively, leaf area plasticity, and WUE_i, as the negative logarithm of the p-value. Dashed lines depict an arbitrary threshold for significance that is consistent across comparisons. (C) Transcriptomic association with plastic leaf area responses to drought and WUE_i. Spearman's rank correlation depicts the relationship between the association of the transcript abundance of each gene in the Arabidopsis genome with leaf area plasticity in response to drought (r_s) on the y-axis and with WUE_i on the x-axis. Dashed lines define an arbitrary threshold to consider transcripts correlated positively ($r_s \geq 0.4$) or negatively ($r_s \leq -0.4$) associated with leaf area plasticity (y-axis) or WUE_i (x-axis). *CBF5* and *CNGC16* exemplify transcripts with opposing relationships to leaf area plasticity and water use efficiency as shown in 4C, D and E. Scatter plots depicting the relationship (P-value < 0.05) between leaf area plasticity index in response to drought (4D), or water use efficiency (4E) on the y-axis, and transcript abundance (FPKM) of *CBF5* on the x-axis. F and G. Scatter plots depicting the relationship (P-value < 0.05) between (4F) leaf area plasticity index in response to drought or (4G) water use efficiency (Dittberner *et al.*, 2018) on the y-axis, and transcript abundance (FPKM) of *CYCLIC NUCLEOTIDE-GATED CHANNEL 16* (*CNGC16*) on the x-axis. In all panels, data were fitted using a linear regression model. Grey shadow represents the 95% CI of the fit regression line.

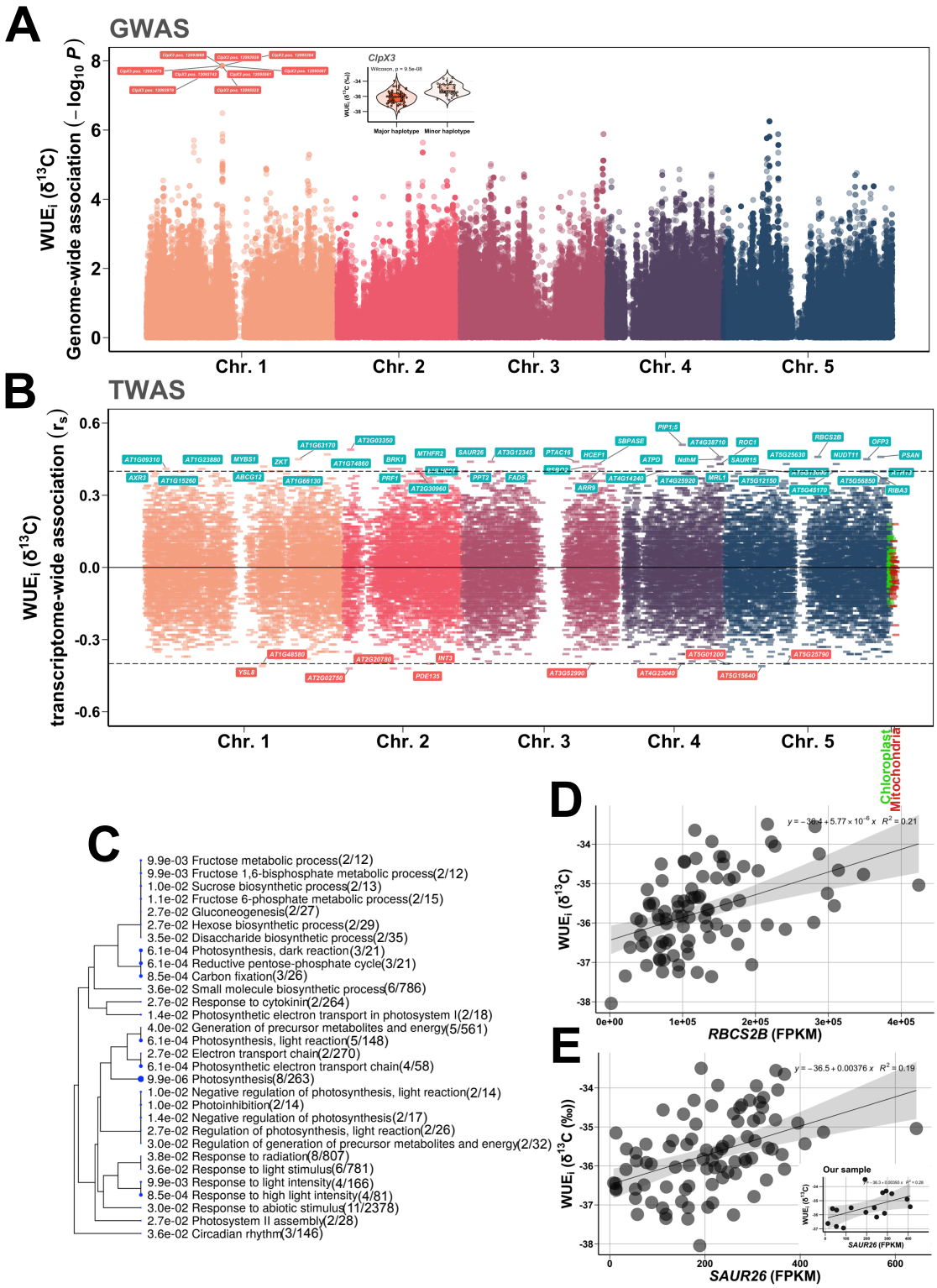

Fig. 6. Photosynthesis-related transcript variants regulate water use efficiency in Iberian Arabidopsis accessions. (A) Manhattan plot representing the genome-wide strength of association between genetic variation and variation in δ13C present within 95 Iberian accessions with δ13C values available from Dittberner *et al*. (2018). The score (y-axis) consists of the negative logarithm of the *P*-value and provides association strength. Inset: Violin plots representing the probability densities of WUE_i for the major and minor allele haplotypes in *ClpX* for the accessions included in Fig. 6A. (B) T-Manhattan plot representing transcriptome-wide strength of association between variation in transcript abundance (Kawakatsu *et al.*, 2016) and natural variation in δ13C. This analysis was performed on all Iberian accessions with both transcript abundance data (Kawakatsu *et al.*, 2016) and δ13C information (Dittberner *et al.*, 2018) (n = 88 accessions). The relationship is defined by the Spearman's rank correlation coefficient (r_s). Dashed lines define an arbitrary threshold for positive ($r_s \geq 0.4$) or negative ($r_s \leq -0.4$) correlation with water-use efficiency (y-axis). Blue labels highlight the transcripts positively associated with higher WUE_i, while red labels highlight those negatively associated with higher WUE_i. (C) Hierarchical clustering tree summarizing the correlation among significant GO Biological Process categories resulting from analysis of the positively correlated candidates resulting from TWA analysis of water use efficiency determined from δ13C values in 88 Iberian Arabidopsis accessions. Ratios provide the number of genes positively correlated with WUE_i within each GO category relative to the total number of genes within that category. The size of the blue dots increases proportionally with P-value significance. (D) Scatter plot depicting the positive relationship (*P*-value < 0.05) between WUE_i (y-axis) and *RuBisCO SMALL SUBUNIT 2B* (*AT5G38420*; *RBCS2B*) transcript abundance (x-axis) for the Iberian accessions included in Fig. 6B. (E) Scatter plot depicting the positive relationship (*P*-value < 0.05) between intrinsic water-use efficiency (WUE_i; y-axis) and *SMALL AUXIN UP RNA 26* (*SAUR26,* AT3G03850) transcript abundance (x-axis) for the Iberian accessions included in 6b. Inset: Scatter plot depicting the positive relationship (*P*-value < 0.05) between intrinsic water-use efficiency (WUE_i; y-axis) and *SMALL AUXIN UP RNA 26* (*SAUR26,* AT3G03850) transcript abundance (x-axis) for the 43 accessions included in our study. For 5D, and 5E, gray shadow represents the 95% CI of the fit regression line (black).